

1 **Molecular compositions and optical properties of dissolved brown carbon in**
2 **biomass burning, coal combustion, vehicle emission aerosols~~in smoke particles~~**
3 **illuminated by excitation-emission matrix spectroscopy and ~~Fourier-transform~~**
4 **~~ion-cyclotron resonance mass spectrometry (FT-ICR MS)~~ analysis**

5 Jiao Tang^{1,4}, Jun Li^{*,1}, Tao Su^{1,4}, Yong Han², Yangzhi Mo¹, Hongxing, Jiang^{1,4}, Min
6 Cui², Bin Jiang¹, Yingjun Chen², Jianhui Tang³, Jianzhong Song¹, Ping'an Peng¹, Gan
7 Zhang^{*,1}

8 ¹State Key Laboratory of Organic Geochemistry, Guangzhou Institute of
9 Geochemistry, Chinese Academy of Sciences, Guangzhou 510640, China

10 ²Department of Environmental Science and Engineering, Fudan University, Shanghai
11 200092, P.R. China

12 ³Key Laboratory of Coastal Environmental Processes and Ecological Remediation,
13 Yantai Institute of Coastal Zone Research, Chinese Academy of Sciences, Yantai
14 264003, China

15 ⁴University of Chinese Academy of Sciences, Beijing 100049, China

16 ***Corresponding authors:** Jun Li (junli@gig.ac.cn); Gan Zhang
17 (zhanggan@gig.ac.cn)

18

19 **Abstract:** Brown carbon (BrC) plays an essential impact on radiative forcing due to
20 its ability to absorb sunlight. In this study, We investigated the optical properties and
21 molecular characteristics fluorescence and chemical structural characteristics of
22 water-soluble and methanol-soluble organic carbon (MSOC) dissolved brown carbon
23 (BrC) in smoke particulates emitted from the combustion of biomass and fossil fuels
24 and vehicle emissions (coal and vehicle exhaust) were investigated by UV-visible
25 spectroscopy, excitation-emission matrix (EEM) spectroscopy and Fourier-transform
26 ion cyclotron resonance mass spectrometry (FT-ICR MS) coupled with electrospray
27 ionization (ESI). The results showed that these smoke aerosols of biomass burning
28 (BB) and coal combustion (CC) had a higher mass absorption efficiency at 365 nm
29 (MAE₃₆₅) than that of vehicle emissions. A stronger MAE₃₆₅ value was also found in
30 MSOC than water-soluble organic carbon (WSOC), indicating low polar compounds
31 would possess higher light absorption capacity. Parallel factor analysis (PARAFAC)
32 identified six types of fluorophores in the WSOC including two humic-like substances
33 (HULIS-1) (P1, and P6), three protein-like substances (PLOM) (P2, P3, and P5), and
34 one undefinition (P4). HULIS-1 was mainly from aging vehicle exhausts, P2 was only
35 abundant in BB aerosols, P3 was ubiquitous in all tested aerosols, P4 was abundant in
36 fossil burning aerosols, and P5 was more intense in the fresh vehicle-exhaust particles.
37 The MSOC chromophores (six components, C1-C6) exhibited consistent
38 characteristic with WSOC, suggesting the method could be used to indicate the
39 origins of chromophores. FI-ICR mass spectra showed that CHO and CHON were the
40 most abundant components of WSOC, but S-containing compounds appeared a higher
41 abundance in the CC aerosols and vehicle emission than BB aerosols. While
42 considerably low S-containing compounds with largely CHO and CHON were
43 detected in MSOC. The unique formulas of different sources determined by the Venn
44 diagram presented different molecular distribution. To be specific, BB aerosols with
45 largely CHO and CHON had a medium H/C and low O/C ratio; while, CC aerosols
46 and vehicle emission with largely S-containing compounds had an opposite H/C and
47 O/C ratio. Moreover, the light absorption capacity of WSOC and MSOC was
48 positively associated with the unsaturation degree and molecular weight in the source

49 aerosols. The above results are potentially applicable to further studies on EEM-based
50 or molecular characteristic-based source apportionment of chromophores in
51 atmospheric aerosols.

52

53 ~~Six components were resolved by parallel factor analysis (PARAFAC) of the~~
54 ~~water soluble and methanol soluble organic carbon (MSOC) fractions, respectively.~~
55 ~~These fluorescent components varied among sources. Combined with FT-ICR MS ion~~
56 ~~groups, we found that the fluorescent components agreed well with the functional~~
57 ~~groups, particularly with nitrogen (N) and sulfur (S) containing groups. Among the~~
58 ~~six PARAFAC components (P1–6) retrieved from the water soluble organic carbon~~
59 ~~(WSOC) fraction, except for the P3 component, the other components exhibited~~
60 ~~different values among the three types of emission sources tested. Vehicle exhaust was~~
61 ~~characterized by high P1 and P6 components, which are mainly associated with~~
62 ~~aromatic organosulfate compounds, and a high P5 component, mainly associated with~~
63 ~~sulfonates; coal combustion was characterized by a high P4 component, which is~~
64 ~~associated with nitrooxy organosulfate (nitrooxy OS) compounds; and biomass~~
65 ~~burning was characterized by the P2 component. Similar results were observed in the~~
66 ~~case of the MSOC fraction. This study reveals the source contribution and possible~~
67 ~~structures of previously unclear excitation emission matrix (EEM) fluorescent~~
68 ~~components in combustion derived aerosols. These are the first findings of this type~~
69 ~~and are potentially applicable to further studies on EEM-based source apportionment~~
70 ~~of dissolved BrC in aerosols.~~

71

72 **1 Introduction**

73 Carbonaceous aerosols play an important role in the Earth's radiative balance. One
74 such aerosol, black carbon (BC), absorbs significant amounts of light and exerts a
75 warming effect, while organic carbon (OC) was initially thought to only scatter solar
76 radiation (Wong et al., 2017; Mo et al., 2017; Saleh et al., 2014). However, recent
77 studies show that there are certain types of OC that absorb radiation efficiently in the
78 near ultraviolet (UV) (300–400 nm) and ~~UV-visible (UV-Vis)~~ ranges, which are called
79 brown carbon (BrC). ~~They can and are~~ able to positively shift the net direct radiation
80 forcing (DRF) (Saleh et al., 2014; Laskin et al., 2015; Kirchstetter and Thatcher, 2012).
81 According to a simulation model, the inclusion of BrC may enhance total aerosol
82 absorption by 7–19% (Feng et al., 2013). According to previous study, BrC in
83 atmospheric aerosols mainly originates from emissions from biomass burning (BB)
84 and ~~fossil fuel combustion, coal combustion (CC), vehicle exhausts,~~ and the formation
85 of secondary organic aerosol (SOA) (Zhu et al., 2018; Laskin et al., 2015 Xie et al.,
86 2017; Kumar et al., 2018). Among ~~the various sources listed above them,~~ primary
87 emissions contributed significantly to BrC absorption (Fan et al., 2012; Yan et al.,
88 2015; Zhang et al., 2011). Recently, many studies have investigated the optical
89 properties and molecular characteristic of BrC in laboratory simulated combustion
90 (Budisulistiorini et al., 2017; Lin et al., 2018; Lin et al., 2016; Song et al.,
91 2019)chemical and optical properties of BrC in smoke particles emitted from biomass
92 burning, coal combustion in a control laboratory chamber –and their light absorption
93 in controlled emissions characteristic of vehicle emissions (Xie et al., 2017)-. However,
94 there were no available studies on the comprehensive characteristic of BrC in various
95 sources and their variations in optical and chemical information impacted by these
96 sources, therefore, investigating the BrC in different sources would improve our
97 understanding of the evolution of BrC absorption.

98 ~~–However, most studies mainly focused on light absorption of BrC; little~~
99 ~~structural information is available.–~~

100 Excitation-emission matrix (EEM) spectroscopy can provide structure information of
101 chromophores, and thus has been widely applied to identify the sources and chemical

102 nature of chromophoric dissolved organic matter (CDOM) in aquatic environments
103 since the 1990s (Shimabuku et al., 2017;Wells et al., 2017;Bhattacharya and Osburn,
104 2017;Coble, 1996), ~~while few studies have focused on the fluorescence properties of~~
105 ~~chromophores in atmospheric environments. Recently, many studies have suggested~~
106 ~~that the~~Due to the optical properties of chromophoric water-soluble organic carbon
107 (WSOC) in the atmosphere ~~was/were~~ similar to CDOM in aquatic environments (Qin
108 et al., 2018;Fu et al., 2015; Graber and Rudich, 2006), ~~and~~ this technique could ~~be~~
109 ~~extended~~ to atmospheric research. It has to be mentioned that ~~Fluorescence~~
110 fluorescence is a radiative process that occurs between two energy levels of the same
111 multiplicity (Andrade-Eiroa et al., 2013). Generally, ~~C~~compounds with rigid planar
112 structures and highly conjugated systems have intrinsic fluorescence emission
113 characteristics and are important BrC chromophores, such as aromatic acids, phenols,
114 nitroaromatics, polycyclic aromatic hydrocarbons (PAHs), quinones, and so on, ~~which~~
115 ~~are important BrC chromophores~~ (Lin et al., 2018;Zhang et al., 2013). ~~Furthermore,~~
116 ~~Laskin et al. believed that fluorescence is sensitive to the molecular (or~~
117 ~~supramolecular) identity of BrC compounds and anticipated that fluorescence-based~~
118 ~~methods will become increasingly important in the study of BrC. Therefore,~~
119 chromophores in Fluorescence-fluorescence spectra, ~~which are~~ could be considered a
120 “fingerprinting” tool, especially when combining it with parallel factor (PARAFAC)
121 analysis which can decompose EEMs signal into their underlying chemical
122 components (Murphy et al., 2013).~~have been applied to organic aerosols. Chen et al.~~
123 For instance, ~~(Chen et al., (2016b) observed that the fluorescence spectra of~~
124 water-soluble extracted organic matter chromophores identified by PARAFAC from
125 the urban, forest, and marine aerosols were varied ~~depending on~~with the sampling
126 sites and periods, and were affected by oxidative and functional groups. ~~Lee et al.~~(Lee
127 et al., (2013) ~~reported-illustrated~~ that SOA derived from the oxidation of limonene and
128 decene with O₃ and OH had presented different fluorescence spectra. Therefore, BrC
129 characteristics from various sources may differ. The biggest challenge wWhen
130 analyzing chromophoric BrC using fluorescence spectra, however, is the lack of a
131 classification system for fluorescence spectra, to distinguish chromophores from ~~the~~

132 ~~majority of most~~ non-absorbing constituents and to determine the chemical structures
133 of the chromophores.

134 ~~The combination of~~ Fourier-transform ion cyclotron resonance mass spectrometry
135 (FT-ICR MS) coupled with electrospray ionization (ESI) ~~and EEM~~ is a powerful
136 platform for the detailed characteristics investigation of organic material at the
137 molecular level, characterizing BrC chromophores, and is expected to enable us to
138 deduce the molecular compositions of these chromophores. With the advantage of
139 ultrahigh-resolution, the accuracy of mass measurements, and high sensitivity (Feng
140 et al., 2016), FT-ICR MS has been successfully used to characterize organic aerosol
141 (Jiang et al., 2016; Song et al., 2018; Mo et al., 2018), cloud water (Zhao et al., 2013),
142 and natural organic matter (Sleighter et al., 2012; Feng et al., 2016). For example, a
143 relative study determined their molecular families of dissolved organic matters
144 (DOMs) associated with fluorescent components by using FI-ICR MS (Stubbins et al.,
145 2014), which could provide more chemical information of chromophores. The
146 ultrahigh resolution, accuracy of mass measurements, and high sensitivity make this
147 technique suitable for studying complex mixtures at the molecular level, and for
148 identifying the chemical compositions of the substances being studied with a high
149 degree of confidence (Feng et al., 2016).

150 Residential ~~coal combustion~~CC and ~~biomass burning~~BB emissions, and motor
151 vehicle emissions are significant anthropogenic sources of air pollutants,
152 exceptionally fine particulate matter (PM_{2.5}) on urban and regional scales (Gentner et
153 al., 2017; Yan et al., 2015; Zhang et al., 2018; Chen et al., 2015). ~~are very important~~
154 ~~anthropogenic sources of air pollutants, especially fine particulate matter (PM_{2.5}), in~~
155 ~~China (Tian et al., 2017).~~ ~~Concerns about the environmental and health effects of~~
156 ~~vehicle emissions have existed for decades (Dai et al., 2015).~~ The characteristics of
157 BrC from these origins may differ to those of BrC from other sources. In this study,
158 to obtain a comprehensive understanding of BrC originating from different sources,
159 UV-vis, EEMs, and FI-ICR MS analysis were performed for water-soluble and
160 methanol-soluble organic carbon (MSOC) from the smoke particles of simulated
161 combustion of biomass fuels and coals, and vehicle emission aerosols. Statistical

162 analysis of PARAFAC was applied to EEM spectra to resolve the fluorescent
163 compounds. All, and unique molecular characteristic of water-soluble organic carbon
164 (WSOC) and MSOC were analyzed and discussed on the base of FI-ICR MS.
165 Relationship between optical properties and chemical structures were discussed by
166 using linear regression coefficient.~~we investigated the solvent extractions of organic~~
167 ~~compounds with different polarities from the smoke particles of simulated combustion~~
168 ~~emissions from biomass fuel, coal, and vehicles, and characterized their optical~~
169 ~~properties in terms of UV-Vis absorption and excitation-emission matrix (EEM)~~
170 ~~spectra. We employed FT ICR MS coupled with ESI to investigate the molecular~~
171 ~~compositions of the fluorescent components identified by parallel factor analysis~~
172 ~~(PARAFAC). We also aimed to identify the possible chemical structures of these~~
173 ~~chromophores and create a source library of BrC chromophores for applications to~~
174 ~~atmospheric BrC apportionment based on fluorescence technology.~~

175 **2 Experimental methods**

176 **2.1 Sample collection and preparation**

177 The smoke particles were collected by the instrument coupled with dilution channel
178 which was designed to simulate fire emissions representative of “real-world” open
179 ~~biomass burning~~BB and household ~~coal combustion~~CC activities (Figure S1). In the
180 present study, a total of 27 ~~biomass burning~~BB samples (IDs:-1-27) were collected at
181 Xishuangbanna city, Yunnan Province, from May 20th to June 3th, 2016 and the
182 detailed sampling process was described in our previous article (Cui et al., 2018). In
183 short, raw fuels (rough 20×3×2 cm³) were air-dried for several days, and ignited in a
184 ~~stainless~~-stainless-steel bowl, and then the rising smoke was collected through a
185 dilution system. The sampling system mainly consisted of a dilution tunnel, a
186 residence time chamber, three particulate matter (PM) samplers, and so on. Every
187 biomass was burned three times, about 1-2 kg fuels per burn. Every combustion
188 process lasted for 20 minutes.~~Every biomass about 1-2 kg fuels was burned three~~
189 ~~times, and each combustion process lasted for 20 minutes.~~ The collection of smoke

190 particle started when fuel ignited, and end until the concentration of CO₂ down to
191 atmosphere CO₂ level. Dilution ratios of each experimental process were calculated
192 using the CO₂ concentrations before and after dilution. The collection flow rate and
193 average dilution ratio were 180 L/min and 2.1, respectively. And the other 6 ~~biomass~~
194 ~~burningBB~~ samples (IDs: ~~28-33~~) were collected at Guangzhou city, Guangdong
195 Province.

196 The smoke particles of ~~coal-combustionCC~~ (IDs: ~~34-50~~) were collected as same
197 as that of ~~biomass-burningBB~~ experiment, but used a stove, ~~at-in~~ Guangzhou city,
198 Guangdong province, from Nov ~~_~~18th, 2017 to Jan 23th, 2018. The tested stove is
199 technically improved stoves (named Jin-Yin stove). Due to the difficulty of ignition of
200 coal, we used smokeless charcoal to ignite one-third (about 300 g) of the raw-coal
201 chunk (2-5 cm in size) in ~~the~~ stove, removed the charcoal after ignition, and then
202 added the remaining raw-coal chunk (about 700 g) to start to collect the smoke
203 particle. ~~Every coal was also burned three times, about 1 kg fuels per burn. Every~~
204 ~~combustion process lasted for about 40-150 minutes. Every coal about 1 kg fuels was~~
205 ~~burned three times, and each combustion process lasted for about 40-150 minutes.~~
206 The collection flow rate and average dilution ratio were 150 L/min and 1.5,
207 respectively. Additionally, a modified combustion efficiency (MCE) was calculated to
208 characterize the relative amount of smoldering and flaming combustion phase (Lin et
209 al., 2016; Cui et al., 2018). The average MCE values were 0.73 ± 0.08 for ~~coal~~
210 ~~combustionCC~~ experiment, ~~—~~ but unavailable for ~~the biomass-burningBB~~ experiment
211 because the CO sensor did not work in the field work which was mentioned in our
212 previous paper (Cui et al., 2018).

213 ~~Tunnel aerosols (total eight samples, IDs51-58) Eight tunnel samples (IDs: 51-58)~~
214 were collected at Siping Tunnel from Nov 1th to 2th, 2017 and Xiaoyangshan Tunnel
215 from Dec 1th to 2 th, 2017, in Shanghai city, as well as ~~two vehicle exhaust particles~~
216 ~~(IDs59-60)two vehicle exhaust samples (IDs: 59-60)~~ were collected from ~~the direct~~
217 ~~emission of two different trucks (more fresh aerosols). With no other instructions,~~
218 ~~vehicle emissions represented all tunnel aerosols and vehicle exhaust particles.~~ The
219 filters were wrapped in aluminum foil and pre-baked at 450 °C for 5 hours before

220 sampling—_and stored at -20 °C after sampling. ~~Overall, There there~~ were a total of
221 60 total suspended particulate matter (TSP) samples on source emissions in the
222 ~~currentis experimentstudy~~, and blank samples ~~which that~~ were collected at different
223 times and locations were used for correcting filter samples.

224 WSOC for UV-Vis absorption and EEM analysis was extracted with purified
225 water (resistivity of >18.2Ω) via ultra-sonication of quartz filter punches for 30
226 minutes. ~~Because water cannot effectively extract the BrC (Liu et al., 2013;Shetty et~~
227 ~~al., 2019), the remaining filter was further freeze-dried and extracted with methanol~~
228 ~~(HPLC grade) to~~After the extraction, we obtained the ~~methanol-soluble-organic~~
229 ~~carbon (MSOC)-~~constituent ~~for better understand the optical properties and molecular~~
230 ~~composition of BrC. by freeze drying the water extracted filter and performing~~
231 ~~ultrasonic extraction with methanol (HPLC grade) in the same manner. It is worth~~
232 ~~Note-noting~~ that the MSOC ~~fraction-of-the-methanol-extract~~ in ~~our-currentthis~~ study
233 ~~are-is~~ not necessarily ~~similar tolike~~ those of the same names in other studies. All ~~the of~~
234 ~~the~~ extracts were filtered through a 0.22 μm polytetrafluoroethylene membrane into
235 amber colored glass vials to remove the insoluble material.

236 2.2 Carbon analysis

237 We measured both OC and elemental carbon (EC) using an aerosol carbon analyzer
238 (Sunset Laboratory, Inc., USA), following the NIOSH thermal-optical transmittance
239 (TOT) standard method (Mo et al., 2017), and the emission factors (EFs) of PM, OC
240 and EC were calculated and detail information was presented in supplement. We also
241 analyzed the elemental compositions of biomass (C, H, O, and N) and coal (C, H, O,
242 N, and S) using an elemental analyzer (vario EL cube; Elementar, Germany) and the
243 results were listed in Table S1 and S2. The carbon content of WSOC were measured
244 using total organic carbon analysis (Vario TOC cube; Elementar) before acidifying
245 with phosphoric acid to remove inorganic carbon, while that of the MSOC ~~fractions~~
246 ~~were-was~~ assessed using the method developed by ~~Chen-et-al-a previous study~~ (Chen
247 et al., 2017b). In short, the extracted MSOC ~~fraction~~ was dried gently under nitrogen,
248 and then re-dissolved in 500 μL methanol. Subsequently, 50 μL of the solution was

249 added to the clear quartz filter (area: 1.5 cm²) until dry, and analyzed using the TOT
250 standard method.

251 **2.3 UV–Vis absorption spectra and EEM fluorescence spectra**

252 The UV-vis absorption and ~~absorption and~~ EEM spectra of ~~the~~ WSOC and MSOC
253 ~~samples~~ were analyzed using a UV-Vis spectrophotometer (UV-4802; Unico, China)
254 and an Aqualog fluorometer (Horiba Scientific, USA), respectively. The wavelengths
255 used to characterize the UV-~~Vis-vis~~ spectra were between 200 to 800 nm at a step size
256 of 2 nm. Purified water was used as a baseline correction before measure. Mass
257 absorption efficiency (MAE, m² g⁻¹ C) ~~can be~~ was obtained as following equation (Li
258 et al., 2018):

$$259 \quad MAE_{\lambda} = A_{\lambda} \cdot \ln(10) / (C \cdot L) \quad (1)$$

260 Here, A_{λ} is the value of light absorption at given wavelength given by the
261 spectrophotometer; C ($\mu\text{g C mL}^{-1}$) is the concentration of WSOC and MSOC ~~fractions~~;
262 L is the optical path length. Moreover, the pH of WSOC ~~fraction~~ was measured for all
263 samples within the range of 5.5-6.5, generally thought it ~~didn't~~ did not affect the
264 absorbance according to prior study (Chen et al., 2016a).

265 The emission and excitation wavelengths of the fluorescence spectra were from
266 245 to 580 nm and 240 to 500 nm, respectively. The wavelength increments of the
267 emission and excitation scans were 4.66 and 3 nm, respectively. Further, we
268 subtracted the contributions of the solvents to the fluorescence spectra.

269 **2.4 Ultrahigh resolution ESI FT-ICR MS analysis**

270 The WSOC and MSOC of six selected samples including two BB aerosols (Musa and
271 Hevea), two CC aerosols (a anthracite and bituminous coal), one day of tunnel aerosol
272 (combined the aerosols in inlet and outlet of the tunnel in the same day, TA), and one
273 vehicle exhaust particles were analyzed using FT-ICR MS. Two fractions of six
274 samples (IDs: 18 and 23 represented the mean fluorescence level of biomass burning;
275 IDs: 38 and 46 represented anthracite and bituminous coal, respectively; IDs: 55
276 represents a day's worth of samples of tunnel inlet and outlet, and IDs: 59 represents

277 ~~direct vehicle exhaust) were selected for FT-ICR MS analysis.~~ To remove inorganic
278 ions ~~prior to before~~ instrumental analysis, ~~the WSOC fraction~~ was further adjusted to
279 pH = 2 by the addition of hydrochloric acid (HCl); and then passed through a
280 solid-phase extraction cartridge (Oasis HLB, 30 μ m, 60 mg/cartridge; Waters
281 Corporation, USA). The constituent retained on the SPE cartridge were eluted with
282 methanol containing 2% ammonia (v/v). Eluted samples were evaporated until dry
283 under a gentle nitrogen gas stream. The extracted solutions by methanol was ~~also~~
284 evaporated under a gentle nitrogen gas stream for preparation.

285 We used the analysis method of FT-ICR MS described in detail in ~~one of our~~
286 previous ~~studies study~~ (Mo et al., 2018). Briefly, ~~ultrahigh-ultrahigh~~-resolution mass
287 spectra were obtained using a solarix XR FT-ICR MS (Bruker Daltonics GmbH,
288 Bremen, Germany) equipped with a 9.4-T superconducting magnet and an ESI ion
289 source. The system was operated in negative ionization mode. The ion accumulation
290 time was set to 0.6 s. The lower and upper mass limit was set to m/z 150 and 800 Da,
291 respectively. The mass spectra were externally calibrated with arginine clusters using
292 a linear calibration and then internally recalibrated with typical O₆S₁ class species
293 peaks using quadratic calibration in DataAnalysis ver. 4.4 software (Bruker Daltonics).
294 A typical mass-resolving power >450 000 at m/z 319 with <0.2 ppm absolute mass
295 error was achieved. The mass spectra of field blank filters were analyzed to detect
296 possible contamination following the same procedures. More data processing was
297 presented in S1 of supplement.

298 **2.5 PARAFAC analysis for EEM spectra**

299 ~~Parallel factor (PARAFAC)~~ analysis with non-negativity constrains was used to
300 explore the fluorescent components in dissolved BrC based on the method established
301 by Murphy et al (Murphy et al., 2013;Andersson and Bro, 2000), which was
302 performed using drEEM toolbox version 2.0 using a MATLAB software
303 (<http://models.life.ku.dk/drEEM>). This method had been widely applied to the
304 analysis of fluorescence spectra in aerosol (Chen et al., 2016b;Chen et al.,
305 2016a;Matos et al., 2015;Wu et al., 2019). Absorbance measurements was used to

306 correct the EEMs for inner filter effects (IFE) according to the previous studies
307 (Luciani et al., 2009;Gu and Kenny, 2009;Fu et al., 2015). The highest light
308 absorbance in the calibrated wavelength range ~~of WSOC and MSOC in two fractions~~
309 was not greater than 2 (mostly below 1 at 254 nm), which is appropriate for the inner
310 filter corrections of the EEMs (Gu and Kenny, 2009;Murphy et al., 2013). Each EEM
311 was normalized to the Raman peak area of purified water collected on the same day to
312 correct fluorescence in Raman Units (RU) at excitation 350 nm, ~~and~~ and corrected for
313 the dilution factor (Murphy et al., 2013;Murphy et al., 2010). Additionally, the signals
314 of the first-order and second-order Rayleigh and Raman scattering in the EEM were
315 removed by ~~using~~ an interpolation method (Bahram et al., 2006). Repeated
316 convergence of the model was examined based on the iteration of the minimum
317 squares principle. The exploration phases of 2- to 7-component ~~PARAFAC~~ PARAFAC models
318 ~~were~~ contained that evaluation of the shape of spectral loading, leverage analysis,
319 examination of the core consistency, residual analysis, and split half analysis (Figure
320 S2-S7). ~~Finally,~~ ~~s~~ Six component PARAFAC model was identified and successfully
321 passed the split ~~validation analysis~~ with the split style of “S₄C₆T₃” for ~~the~~ WSOC and
322 MSOC ~~fraction~~ in 60 samples, respectively.

323 **3 Results and discussions**

324 **3.1 Emission Characteristics and Optical Properties of Extracts.**

325 The PM, OC, and EC emission factors (EFs) of 27 biomass and 17 coal combustion
326 experiments ~~are~~ ~~were~~ summarized in Table S3. The relevant EFs of some of the
327 biomass species were reported previously (Cui et al., 2018). In ~~the~~ ~~current~~ ~~is~~
328 experiment, the EFs of PM, OC, and EC from burning 27 types of biomass were $15 \pm$
329 $11 \text{ g kg}^{-1} \text{ fuel}$, $8.0 \pm 6.4 \text{ g kg}^{-1} \text{ fuel}$, and $7.7 \times 10^{-1} \pm 3.4 \times 10^{-1} \text{ g kg}^{-1} \text{ fuel}$, respectively.
330 The EFs emitted from bituminous ~~coal combustion~~ ~~CC~~ (PM = $9.1 \times 10^{-1} \pm 6.5 \times 10^{-1} \text{ g}$
331 $\text{kg}^{-1} \text{ fuel}$, OC = $4.2 \times 10^{-1} \pm 3.3 \times 10^{-1} \text{ g kg}^{-1} \text{ fuel}$, EC = $9.4 \times 10^{-2} \pm 1.9 \times 10^{-1} \text{ g kg}^{-1}$
332 fuel) were much higher than those of anthracite combustion (PM = $1.5 \times 10^{-1} \pm 8.9 \times$
333 $10^{-2} \text{ g kg}^{-1} \text{ fuel}$, OC = $1.2 \times 10^{-2} \pm 4.5 \times 10^{-3} \text{ g kg}^{-1} \text{ fuel}$, EC = $1.6 \times 10^{-4} \pm 1.4 \times 10^{-4} \text{ g}$
334 $\text{kg}^{-1} \text{ fuel}$) in the same stove. These differences can be attributed to the high volatile

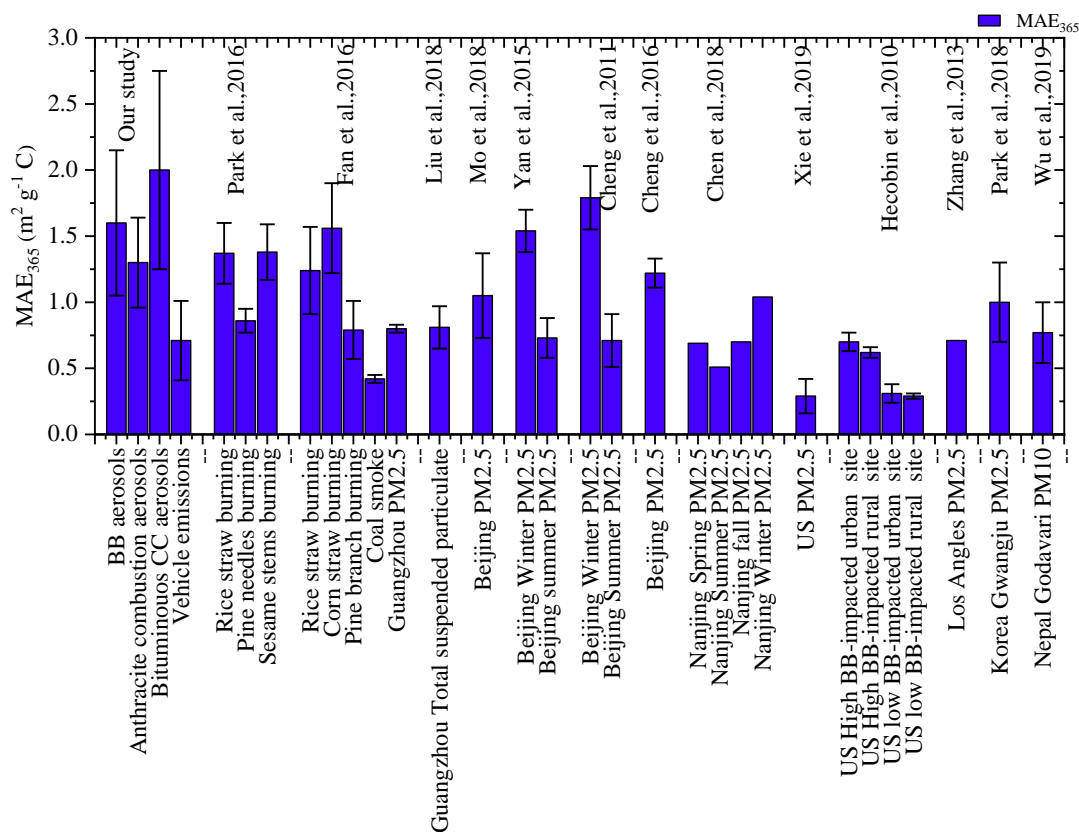
335 matter content of bituminous coal (Tian et al., 2017;Chen et al., 2005). Note that ~~coal~~
336 ~~smoke was collected~~ when the fire had been ignited using ~~one~~ one-third of the
337 material, ~~and then after which~~ the remaining part was added, the CC smoke was
338 collected. Thus, the results of our study ~~were~~would be lower than the real values.

339 ~~Mass absorption efficiency (MAE)~~ can be used to characterize the efficiency of
340 solar energy absorption, which is represented by the degree of conjugation and the
341 amount of electron delocalization in molecules (Chen et al., 2016a). As shown in
342 Figures ~~2b-1 and S8b~~, and ~~in~~ Table S4, MAE at 365 nm (MAE₃₆₅) ~~is~~ was significantly
343 higher in the case of BB and CC aerosols~~biomass burning and coal combustion~~ than
344 in vehicle emissions in the ~~current~~ is study, consistent with the previous findings (Xie
345 et al., 2017;Fan et al., 2016). Bituminous CC aerosols had higher MAE₃₆₅ values than
346 anthracite combustion aerosols. At there, we introduced the EC/OC ratios, which
347 could be used as an indicator of fire conditions (Xie et al., 2017). Figure S8 showed
348 the MAE₃₆₅ of WSOC vs. EC/OC relationships for all BB and CC aerosols. The data
349 clearly showed that the light absorption of BB aerosols was dependent on the burn
350 conditions. However, weak relationship (p>0.05) in CC aerosols suggested another
351 factor may influence the light absorption, such as maturity (Li et al., 2018). Compared
352 to WSOC, Higher-higher MAE₃₆₅ values were observed in the MSOC fractions
353 collected from biomass burningBB (2.3 ± 1.1 m² g⁻¹C) and bituminous coal
354 combustionCC (3.2 ± 1.1 m² g⁻¹C) aerosols. compared to their WSOC fraction values.
355 This ~~may~~ could be due to the fact that these strongly light-absorbing fat-soluble
356 components are likely to be large molecular weight PAHs, and quinones from
357 ~~biomass burningBB~~ and fossil fuel combustion (Sun et al., 2007;Chen and Bond,
358 2010), which were more soluble in low polar solution, while-but we obtained the
359 opposite results in the case of anthracite combustion and vehicle emissions. ~~Moreover,~~
360 ~~the higher MAE₃₆₅ in biomass burning and bituminous coal combustion represented a~~
361 ~~stronger absorbing ability in the case of the MSOC fraction, which reflected greater~~
362 ~~variation in the chemical composition than in the WSOC fraction.~~

363 The MAE₃₆₅ of ~~biomass burning~~ WSOC in this study was compared with the
364 other studies (Figure 1). The BB aerosols in this study had a higher MAE₃₆₅ value

365 than those in controlled BB experiments, while it was comparable to corn straw
366 burning emissions (Park and Yu, 2016;Fan et al., 2016). Besides, the simulated BB
367 aerosols exhibited higher MAE₃₆₅ values than those in highly BB-impacted areas
368 (Hecobian et al., 2010), indicating the aging in the transport process could reduce the
369 light absorption (Dasari et al., 2019). The CC aerosols showed a higher MAE₃₆₅ value
370 than the other coal experiment (Li et al., 2018;Fan et al., 2016), while a comparable
371 value to water-soluble BrC was observed in winter of Beijing (Cheng et al., 2011;Yan
372 et al., 2015). The result indicated the strong influence of BrC in this season in this
373 region. Besides, the simulated combustion aerosols in this study exhibited higher
374 MAE₃₆₅ values than the other areas (such as Guangzhou, Nanjing, Los Angeles,
375 Korea, Nepal, and so on) (see Figure 1).

376 Methanol has a lower polarity than water and can extract the water-insoluble
377 compounds that are generally stronger chromophores. Chen et al., (2017b) extracted
378 organic matters in aerosols using different polar solutions, and they found
379 water-insoluble organic matters (WIOM) had a higher MAE value than the
380 water-soluble organic matters (WSOM), consistent with our result in the BB and
381 bituminous CC aerosols. Vehicle emission aerosols generally had a lower MAE value
382 such as methanol-soluble BrC ($0.62 \pm 0.76 \text{ m}^2 \text{ g}^{-1}\text{C}$) in controlled emission
383 experiment (Xie et al., 2017), which was comparable to WSOC ($0.71 \pm 0.30 \text{ m}^2 \text{ g}^{-1}\text{C}$)
384 but higher than MSOC ($0.26 \pm 0.09 \text{ m}^2 \text{ g}^{-1}\text{C}$) in this study.



385

386 ~~and coal combustion in the WSOC fraction was also higher than that of ambient aerosol and~~
 387 ~~biomass and coal combustion experiments in a laboratory sampling system (Chen et al.,~~
 388 ~~2018; Zhu et al., 2018; Yan et al., 2015; Li et al., 2018; Park and Yu, 2016) (Figure S4). Figure~~
 389 1. Comparison of MAE₃₆₅ in the WSOC fraction of source emission aerosols with the other studies.
 390 The references were as following:(Liu et al., 2018; Mo et al., 2018; Yan et al., 2015; Cheng et al.,
 391 2011; Cheng et al., 2016; Xie et al., 2019; Hecobian et al., 2010; Zhang et al., 2013; Park et al.,
 392 2018; Wu et al., 2019; Fan et al., 2016; Park and Yu, 2016; Chen et al., 2018)

393 3.2 EEM spectra of WSOC and MSOC.~~dissolved BrC.~~

394 Fluorescence spectra was used to characterize the organic chromophores of different
 395 sources. We applied the PARAFAC model (Murphy et al., 2013) to determine the
 396 underlying chromophore components of the 60 emission source samples. Six typically
 397 independent components ~~of in~~ the WSOC fraction were resolved, as shown in the top
 398 of Figure 4-2 and Table 1. Compared with the previous studies, the fluorescence EEM
 399 of P1 and P6 were similar to those for 7CM-C1 (the C1 component of a
 400 seven-component model) and 7CM-C3, named humic-like substances

401 ~~(HULIS-1) pertaining to water extracted matter in urban and forest area, and marine~~
402 ~~aerosols, in Japan~~ (Chen et al., 2016b). Further, there were peaks in the emission
403 wavelengths (> 400 nm) of P1 and P6, which were probably derived from conjugated
404 systems (Chen et al., 2016b). The peak of the P3 component was almost located in
405 region IV, which was categorized as a protein-like (cytidine) or tryptophan-like ~~(peak~~
406 ~~Ⓣ)~~ fluorophore (Qin et al., 2018; Fan et al., 2016). Generally, peaks at shorter
407 excitation wavelengths (< 250 nm) and shorter emission wavelengths (< 350 nm) are
408 correlated with simple aromatic proteins such as tyrosine (Cory and Mcknight, 2005),
409 which is ~~quite~~ similar to the ~~peak fluorescence~~ of ~~the~~ P2 component observed in this
410 study. ~~According to a prior report, the spectra of the~~ P5 component was ~~also~~ similar to
411 tryptophan- and tyrosine-like components (Chen et al., 2017a). ~~Therefore, P2, P3, and~~
412 ~~P5 components were named protein-like substances (PLOM). The spectra of the~~ P4
413 component ~~has been~~ was reported relatively rarely but ~~is~~ similar to previously
414 observed peaks that ~~are~~ were considered to arise mainly in surface water and algal
415 secretions (Yu et al., 2015). ~~It is worth noting~~ Note that the origins and chemical
416 structures of the chromophores studied are not necessarily ~~similar to~~ like those of
417 chromophores with the same names in other types of organic matter.

418 **Table 1.** The maximum excitation and emission wavelengths of the PARAFAC components
419 from the WSOC and MSOC fractions extracted from the three origins

PARAFAC component	Excitation maxima (nm)	Emission maxima (nm)	Assignment according to published papers	References	
WSOC	P1	251, 314	415	HULIS-1, terrestrial humic-like component	(Chen et al., 2016b; Sgroi et al., 2017; Fu et al., 2015)
	P2	254	337	Tyrosine-like	(Cory and Mcknight, 2005)
	P3	287	360	Protein-like (cytidine) or tryptophan-like	(Qin et al., 2018; Fan et al., 2016)
	P4	251	374	-	-
	P5	278	319	Protein-like fluorophores	(Fu et al., 2015)

HULIS-1, conjugated systems, a

P6 254, 371 485 terrestrial humic or fulvic (Chen et al., 2016b)
acid-like component

C1 308 356 -

C2 <250,272 388

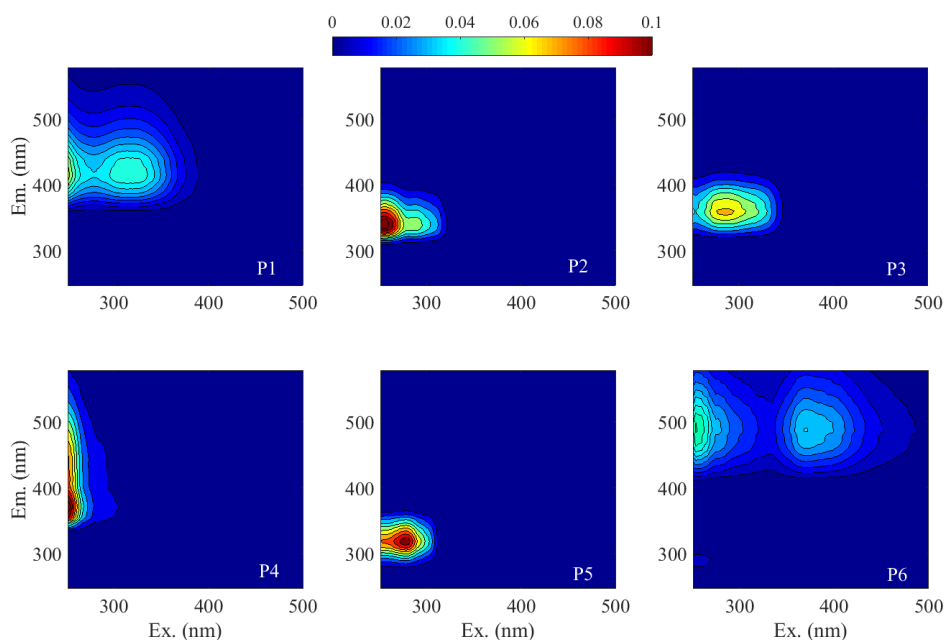
C3 <250 434 C2 for the urban ASOM samples (Matos et al., 2015)

C4 257 360

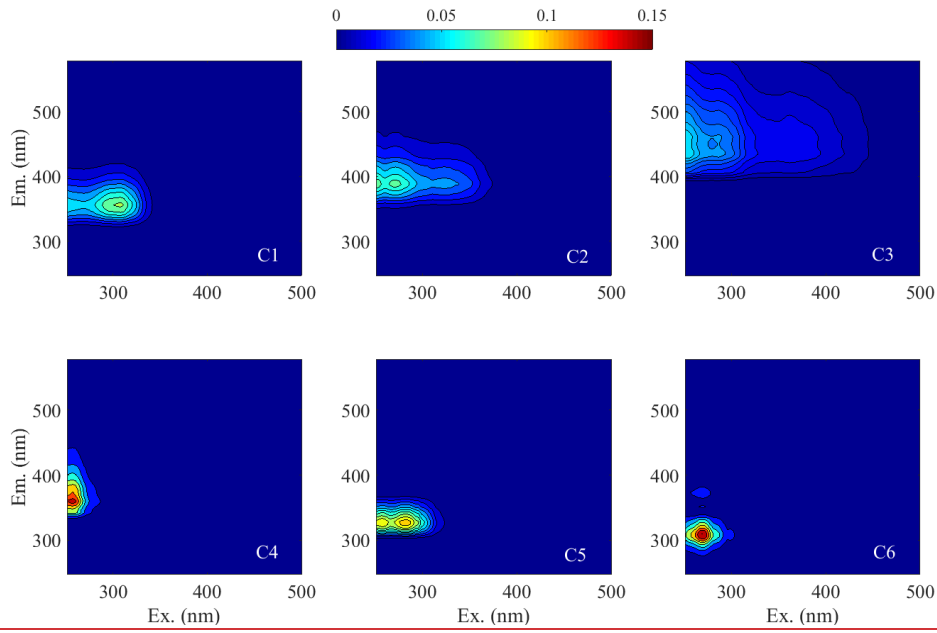
C5 284 328

C6 269 310

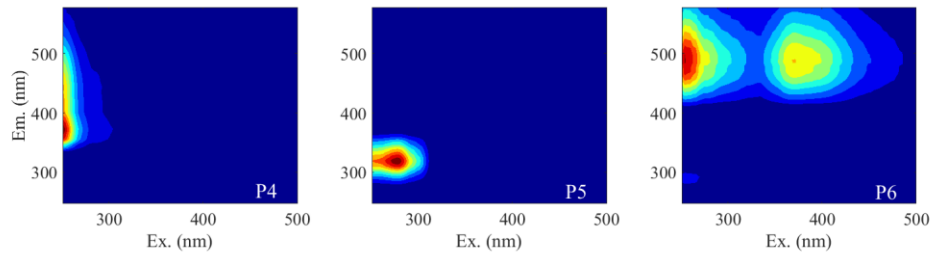
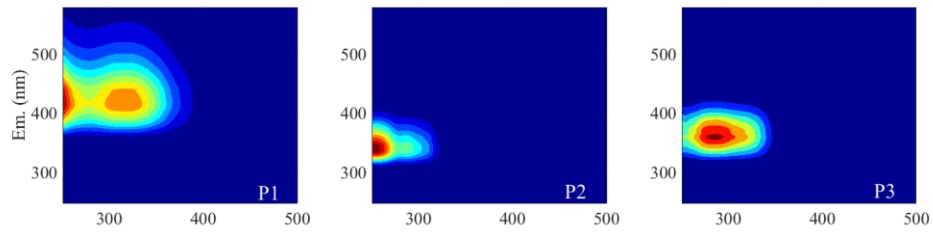
MSOC



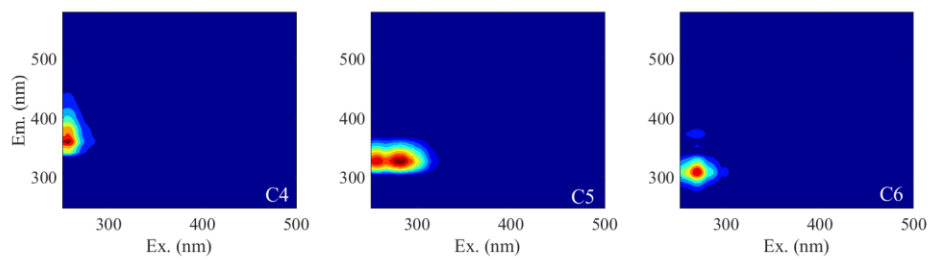
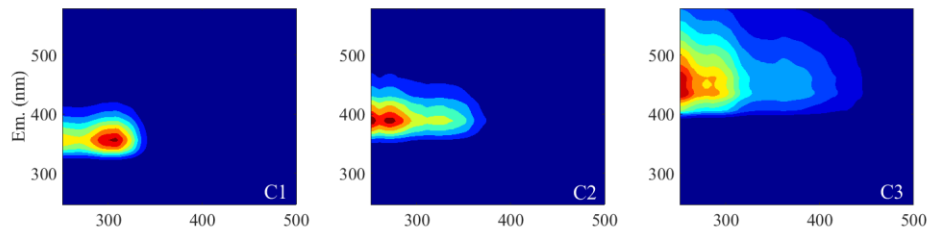
420



421



422



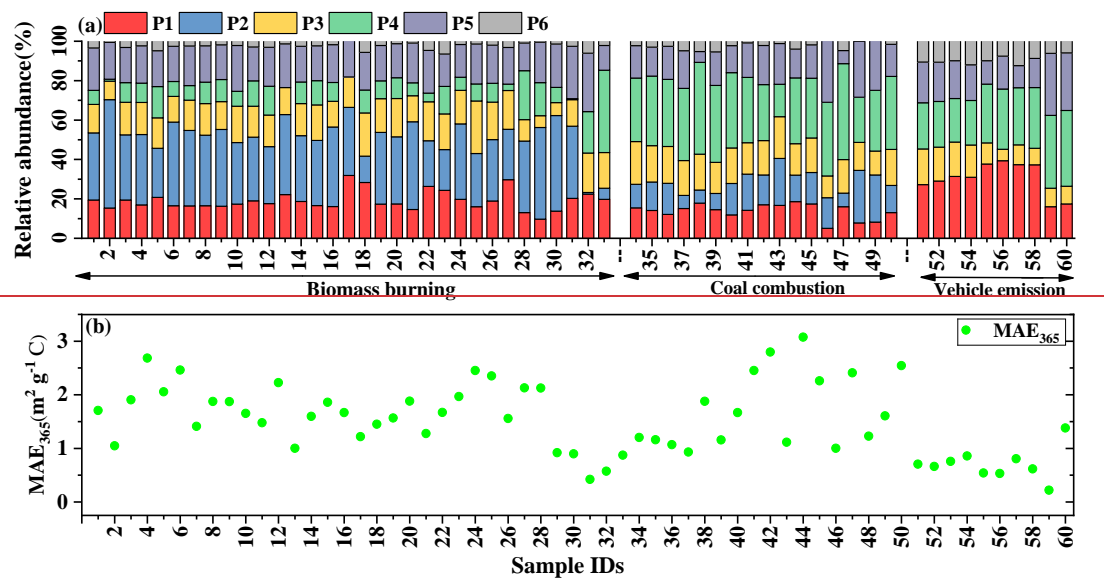
423

424 **Figure 12.** The ~~excitation-emission matrix (EEM) components spectra determined~~ identified by
425 ~~parallel factor (PARAFAC) analysis~~ of WSOC (top: P1-P6) and MSOC (bottom: C1-C6) extracted
426 from three origins.

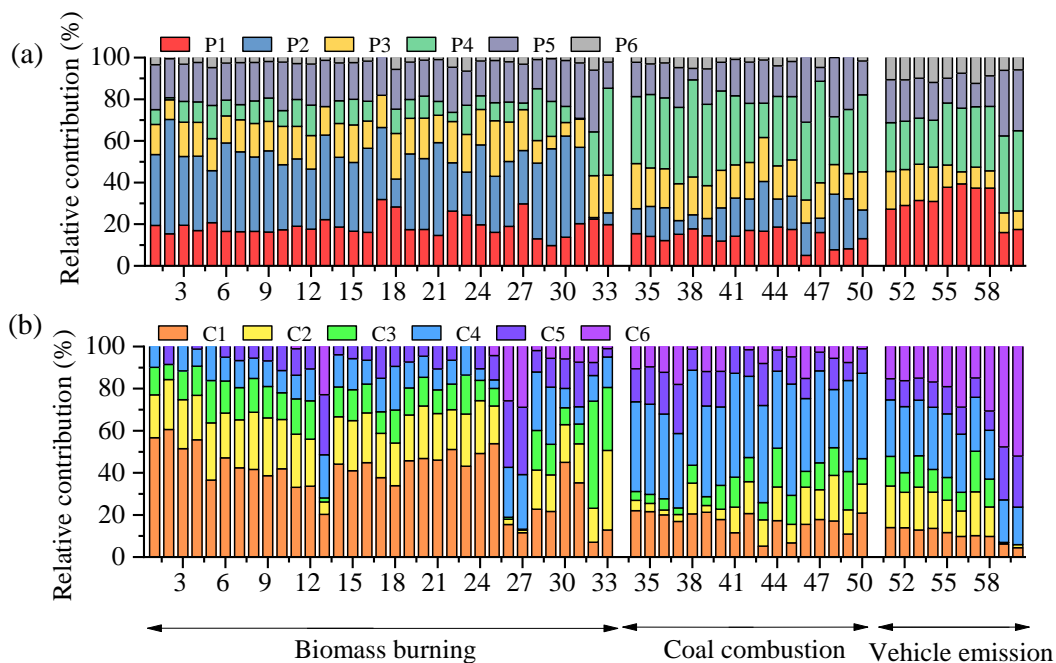
427 The results from the six-component model (abbreviated C1-6) of ~~the~~ MSOC
428 ~~fractions~~ identified by PARAFAC, as described in the bottom of Table 1 and Figure
429 ~~12~~, were ~~obviously~~ different ~~to~~ ~~from~~ those ~~obtained~~ ~~observed in~~ ~~for~~ the WSOC
430 ~~fraction, indicating different chemical structures~~. The peak of C1 component was
431 similar to that of the P3 component of ~~the~~ WSOC ~~fraction~~, but the excitation
432 wavelength was higher ~~than that of P3 component~~, ~~—~~. ~~The higher excitation~~
433 ~~wavelength~~ ~~which~~ indicated the presence of conjugated unsaturated bond systems
434 shifting towards the high wavelengths of ~~the~~ C1 component (Matos et al., 2015).
435 Moreover, as reported ~~in a previous study~~, ~~the~~ C3 component was similar to ~~the~~
436 ~~component~~ C2 ~~component~~ of urban alkaline-soluble organic matter (ASOM) ~~samples~~
437 collected from the city of Aveiro, Portugal (Matos et al., 2015). ~~Because the~~
438 ~~fluorescence spectrum of the MSOC fraction was poorly characterized, the molecular~~
439 ~~composition of the other fluorescent components was studied using FT-ICR MS.~~

440 The maximum fluorescence intensities (F_{\max}) (~~Table S5, S6~~) ~~is~~ ~~was~~ calculated by
441 multiplying the maximum excitation loading and maximum emission loading for each
442 component by its score (Murphy et al., 2013). Generally, changes in the relative
443 abundance of a component ($F_{\max}/\sum F_{\max}$) could indicate changes in its overall
444 importance, which had been successful applied to study the origins of chromophores
445 (Yan and Kim, 2017; Chen et al., 2017a; Chen et al., 2016b; Wu et al., 2019). In the
446 ~~current~~ ~~is~~ study, the relative ~~abundances~~ ~~intensities~~ of ~~different~~ fluorescent components
447 in different types of samples was highly variable, depending on the sources (~~Figure~~
448 ~~3a~~). ~~As shown in Figure 2a~~, P1 component ~~was intense in the case of vehicle emission,~~
449 ~~accounting~~ ~~accounted~~ for an average of ~~30–34~~ \pm ~~84.37~~% of the total fluorescence
450 intensities ~~in the case of tunnel aerosol of vehicle emission~~, ~~—~~, which was higher than
451 ~~BB aerosols (mean \pm SD: 19 \pm 4.8%), CC aerosols (14 \pm 3.8%) and vehicle exhaust~~
452 ~~particles (17 \pm 1.0%). This result indicated P1 component had an aged vehicle exhaust~~
453 ~~origin because a difference of P1 component was observed from tunnel aerosols and~~

454 vehicle exhaust particles. In contrast, the fluorescence of P6 components was weak in
455 any of the samples, but in vehicle emissions ($9.4 \pm 2.3\%$) was higher than BB and CC
456 aerosols (both 2.5%). P5 component was more intense in the vehicle exhaust particles
457 ($30 \pm 1.6\%$) than other sources. P2 and P4 components were was only abundant in the
458 cases of BB aerosols ($33 \pm 11\%$) but did not exhibit in vehicle emissions, suggested
459 some structures responsible for this chromophore could not exist in vehicle emissions.
460 intense in the cases of biomass burning (mean: $33 \pm 11\%$ of fluorescence intensities of
461 biomass burning) and P4 component was the more abundant chromophore in CC
462 aerosols ($34\% \pm 7.7\%$) and vehicle emissions ($29 \pm 5.9\%$), especially in vehicle
463 exhaust particles ($38 \pm 1.1\%$), coal combustion (mean: $34 \pm 7.7\%$), respectively. In
464 contrast, P4 component in BB aerosols was weak ($11\% \pm 7.9\%$), indicating a fossil
465 origin. The P3 components were was almost equal across all samples. The possible
466 reason is was that the P3 components is was similar to the peak of tryptophan-like
467 compounds, where these are which were common to practically all published models
468 and are likely to be found in almost all sources (Yu et al., 2015). It was obvious that
469 P5 component was intense in direct vehicle exhaust (IDs: 59 and 60; mean: $30 \pm$
470 1.6%). In contrast, the fluorescence of P6 components was weak in any of the samples,
471 but the P6 component in vehicle emissions (mean: $9.4 \pm 2.2\%$) significantly exceeded
472 those of biomass burning and coal combustion (both 2.5%). The above results clearly
473 indicates that the chemical composition of chromophoric water-soluble BrC varies
474 remarkably among sources.



475



476

477 **Figure 23.** The relative contribution of each PARAFAC component of WSOC (a) and MSOC (b)

478 in the three source emissions. (a) Relative abundance of each PARAFAC component, (b) mass

479 absorption efficiency at 365 nm (MAE_{365}) values in WSOC fractions from three origins

480 The relative intensities of the fluorescent components in the MSOC fraction exhibited

481 similar characteristics to the WSOC fraction (Figure S8a3b). The C1 and C2

482 components was the substances with more intense in the case of biomass burning BB

483 aerosols (mean: $38\% \pm 14\%$ and $21 \pm 6.9\%$, respectively) than the other sources. C2

484 component was enriched in BB aerosols (21% ± 6.9%) and tunnel aerosols (17% ±
485 6.9%) than those in CC aerosols and vehicle exhaust particles. Also, C2 exhibited a
486 difference between bituminous CC and anthracite combustion aerosols, as well as
487 tunnel aerosols and vehicle exhaust particles, indicating C2 component could be used
488 to identify these sources. C4 components was intense in samples of coal
489 combustion CC aerosols (mean: 41 ± 6.0%) and vehicle exhaust particles (25 ± 4.4%).
490 The levels of component C3 component were was not abundance abundant among
491 between the three sources and not observed in the vehicle exhaust particles,
492 suggesting not a fresh vehicle-exhaust emission origintypes of fuel tested. Instead of
493 C3, The C5 and C6 components was were more intense in directvehicle exhaust
494 particles vehicular exhaust (IDs: 59 and 60; mean: 25 ± 6.8% and 50 ± 6.8%,
495 respectively), suggesting they were more primary vehicle emission chromophores.-
496 The last study observed that the relative abundances of various chromophores in
497 aerosols with different particle sizes were different (Chen et al., 2019). Therefore, the
498 fluorescence technique is sensitive for chromophores with different sources, sizes, and
499 chemical structures and so on. Combining these results with the WSOC mentioned
500 above resultsthe above mentioned WSOC results and comparing the different
501 characteristics and fuel source information, the fluorescent components obtained by
502 EEM-PARAFAC can could potentially assist with the source apportionment of BrC
503 for environmental monitoring applications.

504 3.3 Molecular composition detected by FT-ICR MS

505

506 3.3 Molecular composition of FT-ICR MS and chemical structures of chromophores
507 The relative abundances of the four compound groups (CHO, CHON, CHOS, and
508 CHONS) in the WSOC fraction are presented in Figure S9. These results were
509 consistent with previous results (Song et al., 2018), in which S-containing
510 compounds were mainly found in coal combustion emissions. Conversely, our results
511 proved that N-containing substances were also abundant in coal combustion aerosols.
512 One possible reason for this concerns the viable coal types; for example, significant

513 differences were observed between water extracts of IDs 36 (anthracite coal) and 46
514 (bituminous coal). More detailed information about the molecular compositions is
515 provided in Tables S7 and S8, and Figure S10, S11 and S12.

516 The previous study reported that potential BrC chromophores were identified by
517 determining those compounds in the region between Double bond equivalent (DBE) =
518 $0.5 \times C$ and $DBE = 0.9 \times C$ (in the coordinate axis, the x axis is the C number and the
519 y axis is the DBE value) (Lin et al., 2018). To explore the possible chemical structures
520 of dissolved chromophores, the methods of the O/C and H/C ratios of matter or
521 functional groups were used to classify the ion groups of FT ICR MS as listed in
522 Figure 2. Furthermore, according to the all ions or potential BrC ions, there are total
523 four classifications. The first method is to follow their O/C and H/C ratios of matter to
524 classify all ions of FT ICR MS; the second method is to follow their O/C and H/C
525 ratios of matter to classify potential BrC ions; the third method is to follow their
526 functional groups to classify all ions; the last method is to follow their functional
527 groups to classify potential BrC ions. The relationship between the relative intensities
528 of classified group of ions (the ratio of intensities of each ion group to total ion
529 intensities) and the relative abundance of fluorescent components were presented in
530 Table S9-S16. The results indicated that the method that sorted the potential BrC ion
531 groups by their functional groups is best for explaining the relationship between the
532 chemical composition and fluorescent components. For example, the presence of
533 L-CHON groups with $O/N \leq 2$ suggests that these reduced N compounds may be
534 associated with alkyl amides and alkyl nitrile, as well as heterocyclic aromatic
535 compounds with single N atoms (Alexander et al., 2009; Song et al., 2018). The
536 H-CHON group with $O \geq 3$, $O/N > 2$ and $AI_{mod} > 0.5$ suggests that these compounds
537 contain O and N atoms, such as benzene rings substituted with O-containing groups
538 (hydroxyl, and carboxyl) and nitro-aromatics (Chen et al., 2016b; Song et al., 2018; Lin
539 et al., 2016). The H-CHOS group had $O/S \geq 4$, suggesting the assignment of a sulfate
540 group ($-OSO_3H$). As sulfate groups carry four oxygen atoms and readily deprotonate
541 in ESI, they are more likely to be organosulfates (Jiang et al., 2016). The presence of
542 the H-CHONS group suggested not only the assignment of a sulfate group ($-OSO_3H$),

543 ~~but also an additional one or two nitrooxy groups (-ONO₂) (Mo et al., 2018).~~

544

Table 2. The classification methods of ion groups of FT-ICR MS

Specific classification methods			
Function groups		H/C and O/Ca	
CHO1	O1	Lipids	O/C=0-0.2, H/C=1.7-2.2
CHO>1	O>1	Proteins	O/C=0.2-0.6, H/C=1.5-2.2, N/C ≥ 0.05
L-CHON	O/N ≤ 2	H-Lignin	O/C = 0.1-0.6, H/C = 0.6-1.7, 0.5 < AImod < 0.67
H-CHON	O/N > 2	M-Lignin	O/C = 0.1-0.6, H/C = 0.6-1.7, 0 < AImod ≤ 0.5, DBE ≥ 4
L-CHOS	O/S < 4	L-Lignin	O/C = 0.1-0.6, H/C = 0.6-1.7, 0 < AImod ≤ 0.5, DBE < 4
H-CHOS	O/S ≥ 4	Carbohydrates	O/C = 0.6-1.2, H/C = 1.5-2.2
L-CHONS	O/S < 7(N1); O/S < 10 (N2)	Tannins	O/C = 0.6-1.2, H/C = 0.5-1.5, AImod < 0.67
H-CHONS	O/S ≥ 7(N1); O/S ≥ 10 (N2)	Unsaturated hydrocarbons	O/C = 0-0.1, H/C = 0.7-1.5

545

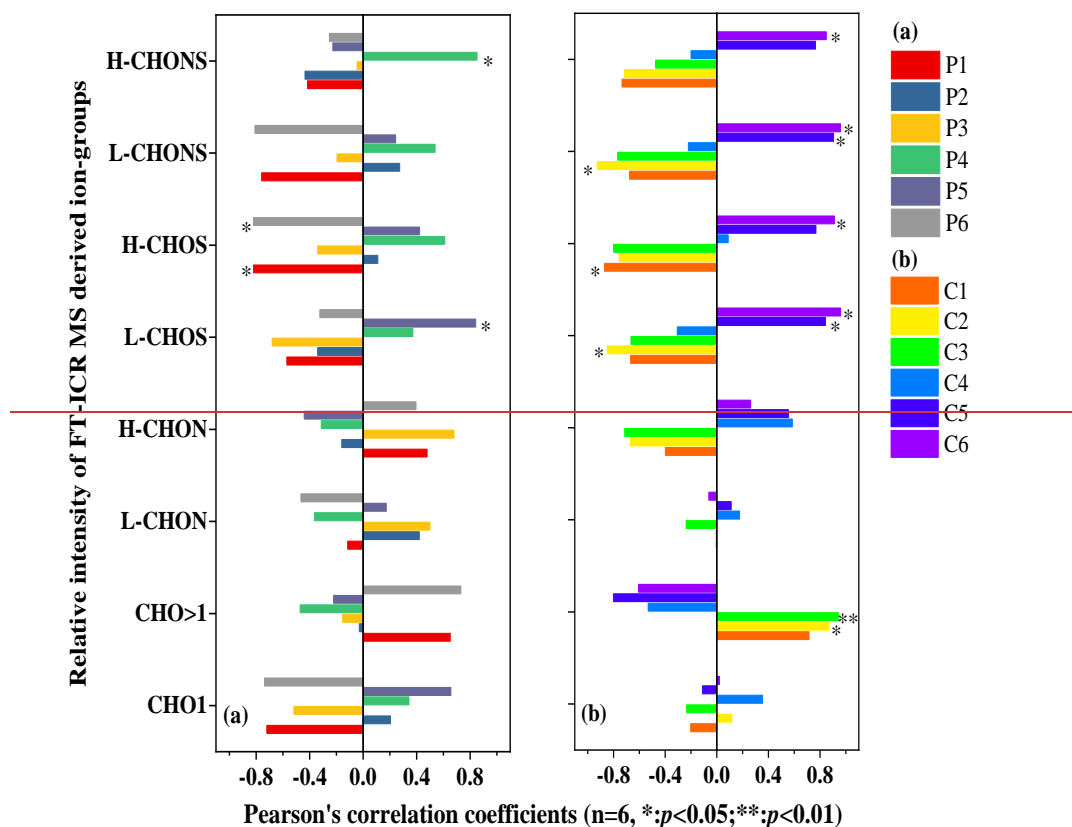
Note that L, M, and H stands for low, moderate, and high, respectively; The lignin group is further divided into three subcategories on the base-

546

of their AImod and DBE (H-Lignin: 0.5 < AImod < 0.67; M-Lignin: 0 < AImod ≤ 0.5, DBE ≥ 4; L-Lignin: 0 < AImod ≤ 0.5, DBE < 4).

547

a: (Patriarca et al., 2018)



549

550

551 ~~Figure 3. Pearson's correlation coefficients (r) and significance levels (two-sided t test)~~
 552 ~~obtained from the correlation analysis between the relative intensity of the ion groups~~
 553 ~~based on Fourier transform ion cyclotron resonance mass spectrometry (FT-ICR MS),~~
 554 ~~and the relative intensity of the (a) six components of the WSOC fractions and (b) six~~
 555 ~~components of the MSOC fractions.~~

556 3.3.1 Composition of chromophores of WSOC

557 ~~The relationship between the relative intensities of the classified ion groups of FT-ICR~~
 558 ~~MS and the relative contents of the PARAFAC components in the WSOC fraction~~
 559 ~~were presented in Figure 3a and Table S15. The P1 and P6 components were both~~
 560 ~~negatively correlated with the H-CHOS group ($p < 0.05$). Considering that P1 and P6~~
 561 ~~components was intense in samples of vehicle emissions, the main compounds~~
 562 ~~detected from this source were O4S1-O12S1 class species with a wide range of C~~
 563 ~~numbers (7-34) and double bonds equivalent (DBE) values (4-20), of which O4S1~~

564 and O5S1 class species, which exhibit an R-OSO₃H structure, were the most
565 abundant. Among these chemical formulas, we found that many aromatic
566 organosulfate isomers with relatively high DBE values (≥ 4) were side chains or
567 aromatic rings, and thus their chemical formulas could be those of alkylbenzene rings
568 substituted with one sulfate and one hydroxyl group (Song et al., 2018), such as
569 C₈H₁₀O₅S (DBE: 4) and C₁₀H₁₀O₆S (6). These structures were detected in
570 humic like substances (HULIS) from coal smoke and SOA generated under all
571 experimental conditions (Riva et al., 2015; Song et al., 2018) and were likely
572 responsible for the P1 and P6 components.

573 The P4 component was positively correlated with the H-CHONS group ($p <$
574 0.05), suggesting nitrooxy organosulfates (nitrooxy OS) (Mo et al., 2018).
575 Nitrooxy OS is probably be formed by photooxidation of biogenic VOCs in smog
576 chamber experiments conducted under high nitrogen oxide (NO_x) concentrations (Lin
577 et al., 2012). These results indicate that coal combustion is an important source of
578 nitrooxy OS, and this conclusion was consistent with the results of previous studies
579 (Song et al., 2018). As shown in Figure 4, a wide range of C number (6–32) and DBE
580 values (3–23) were observed in this group, and the DBE value increased with the C
581 number. The main compounds in this group were O7N1S1–O13N1S1 class species,
582 with O7N1S1 class species being the most abundant. It is worth noting that most of
583 the H-CHONS compounds had DBE values greater than or equal to 4, and the
584 compounds with high intensities in the H-CHONS groups detected from coal
585 combustion were C₆H₅O₇NS (5), C₁₀H₇O₇NS (8), and C₁₀H₆O₁₁N₂S (9). The
586 most likely structure of these compounds is a benzene ring substituted with one
587 sulfate and one or two nitrooxy groups (Song et al., 2018; Jiang et al., 2016). These
588 were also detected in high concentrations in aerosols from Belgium and on a heavy
589 PM_{2.5} haze day in Beijing city (Jiang et al., 2016; Kahnt et al., 2013).

590 The presence of the P5 component was highly correlated with the L-CHOS
591 group ($p < 0.05$). This group was mainly composed of O3S and O7S2 class species
592 from direct vehicle exhaust emissions. Generally, these compounds contained too
593 little oxygen to form sulfate functional groups, containing reduced sulfur (S), such as

594 sulfonates, which was also detected in cloud water (Zhao et al., 2013). In these groups,
595 the main compounds of C₂₆H₂₄O₃S (15), C₂₇H₂₆O₃S (15), and C₂₅H₂₂O₃S (15)
596 were homologues of C₂₄H₂₀O₃S (15), with the same general formula,
597 C_nH_{2n-2}SO₃, and DBE values, of 15, likely corresponding to sulfonates of
598 substituted benzopyrene (C₂₀H₁₂, DBE=15) (Blair et al., 2017). However, the P2 and
599 P3 components were not significantly correlated with these ion groups.

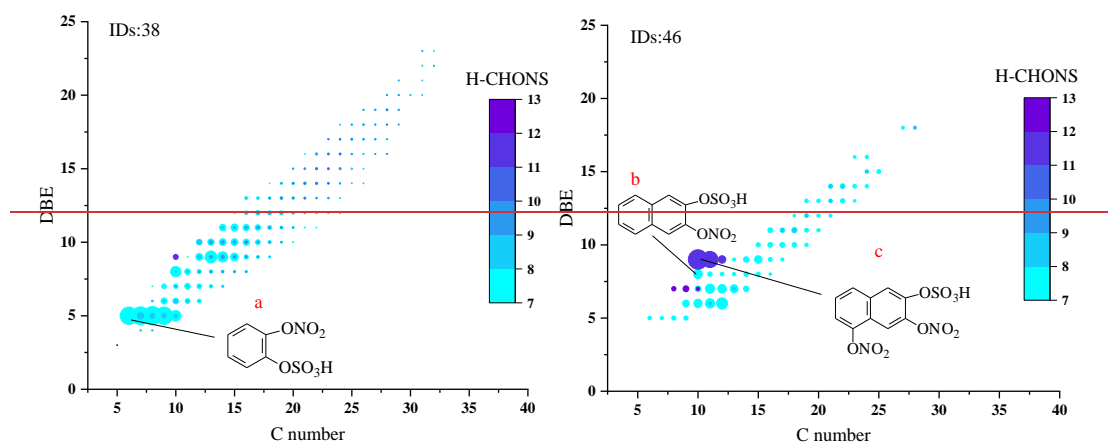
600 3.3.2 Composition of chromophores of MSOC

601 Figure 3b and Table S16 show the relationship between the relative intensity of the
602 classified ions groups and the relative contents of the PARAFAC components of the
603 MSOC fraction. Only the C1 and C3 components were associated with one ion group
604 (H-CHOS and CHO>1, respectively). Considering that the C1 component was highly
605 intense in the case of biomass burning, the H-CHOS groups observed in samples of
606 biomass burning were O5S1, O7S1, O10S2, O13S1 class species, of which O10S2
607 was the most abundant family. The probable structure of these species is an
608 organosulfate with other O-containing functional groups, such as hydroxyl or
609 carboxyl groups. This groups had a narrow range of C numbers (12-16) and DBE
610 values (8), such as C₁₄H₁₄O₁₀S₂ (8) and its homologues C₁₃H₁₂O₁₀S₂ (8);
611 C₁₅H₁₆O₁₀S₂ (8), as well as C₁₅H₁₆O₇S (8), C₁₆H₁₈O₇S (8), C₁₂H₁₀O₁₃S (8);
612 and C₁₃H₁₂O₁₃S (8).

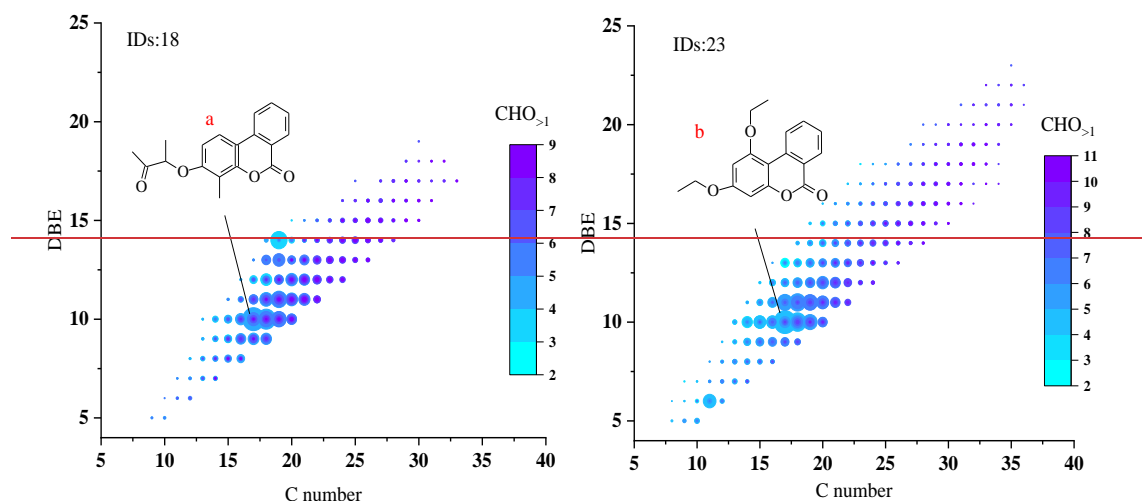
613 C2 component was positively correlated with CHO>1, and negatively correlated
614 with L-CHOS and L-CHONS groups. Figure 5 presented the DBE versus C number
615 for the CHO>1 group from samples of biomass burning, with the main compounds
616 had C numbers of 17-20, DBE (10-11), and O numbers of 4-5. The potential
617 structures of C₁₈H₁₆O₄ (11) and C₁₇H₁₆O₄ (10) are indicated as a and b,
618 respectively, in Figure 5 and are suspected to be cyclic esters. The L-CHOS group
619 were mainly O4S2 class species, of which C₁₂H₁₀O₄S₂ (8) was the main formula.
620 The possible chemical structure is of two S-heterocycles connected to two ester bonds.
621 Thus, C2 components may relate to ester compounds.

622 Further, the C5 component was positively correlated with L-CHOS and
623 L-CHONS groups ($p < 0.05$), and the C6 component was positively associated with

624 all S-containing groups ($p < 0.05$). We list some of the main formulas of these groups
 625 detected in direct vehicle exhaust (IDs: 59), such as $C_{12}H_{12}O_7S_2$ (7) and
 626 $C_{13}H_{14}O_7S_2$ (7) for L-CHOS groups; $C_{14}H_{14}O_{10}S_2$ (8) and $C_{15}H_{16}O_{10}S_2$ (8) for
 627 H-CHOS; $C_{36}H_{23}O_4NS$ (26) for L-CHONS; and $C_{10}H_6O_{11}N_2S$ (9),
 628 $C_{11}H_8O_{11}N_2S$ (9), $C_{10}H_7O_{13}NS$ (8), $C_{11}H_9O_{13}NS$ (8), $C_{12}H_{11}O_{13}NS$ (8) and
 629 $C_{12}H_8O_{14}N_2S$ (10) for H-CHONS. The L-CHOS groups containing two S atoms is
 630 potential to be formed by sulfonation reactions, and their possible structure is of a
 631 fused benzene ring substituted with two sulfonates ($-SO_3H$). $C_{36}H_{23}O_4NS$ may
 632 contain substantial quantities of S-containing compounds with reduced N (e.g., amide
 633 and nitrile, and heterocyclic aromatics) (Song et al., 2018). These results indicate that
 634 the C5 component is potentially related to sulfonates, but the structure of the C6
 635 component is unclear. However, C4 components did not correlate with ion groups.
 636 Note that one class of compounds contributed to several fluorescent components,
 637 which indicated that numerous functional groups affect each component individually.



638
 639 **Figure 4. Double bond equivalent (DBE) versus C number for the H-CHONS group**
 640 **of WSOC of coal combustion samples. The color bar and marker size denote the**
 641 **number of O atoms and the relative intensities of the compounds; a: $C_6H_5O_7NS$**
 642 **(DBE: 5); b: $C_{10}H_7O_7NS$ (8); and c: $C_{10}H_6O_{11}N_2S$ (9).**



643

644 Figure 5. The DBE versus C number for the CHO>1 group of MSOC of biomass
 645 burning samples. The color bar and marker size denote the number of O atoms and the
 646 relative intensities of the compounds, a: C₁₈H₁₆O₄ (11); b: C₁₇H₁₆O₄ (10).

647 The molecular composition of WSOC and MSOC extracted from BB and CC aerosols,
 648 and vehicle emissions were determined by negative ESI-FT-ICR MS. ESI is a soft
 649 ionization method, and it can only ionize polar organic compounds, hydrophilic
 650 molecules (Wozniak et al., 2008), but nonpolar or less polar compounds such as
 651 polycyclic aromatic hydrocarbons (PAHs) and saturated hydrocarbons are not easily
 652 ionized by ESI (Lin et al., 2018). In addition, ESI (-) cannot detect the N-heterocyclic
 653 alkaloid compounds (Laskin et al., 2009). Thus, this study mainly discussed these
 654 easily ionized polar organic compounds by ESI (-).

655 Figure 4 showed the reconstructed negative-ion ESI FT-ICR mass spectra of
 656 WSOC for the six selected samples. Lots of peaks with an intensive mass range
 657 between m/z 150 and 600 were shown in the spectra, with the most massive numbers
 658 of ions within the range of m/z 200-400. Additionally, more formulas were detected in
 659 BB aerosols (total 7708) than CC aerosols (5305) and vehicle emissions (4047) (Table
 660 2), suggesting a higher observed chemical complexity (i.e., the observed peaks).
 661 According to the intensity of each ion, the average molecular formulas of WSOC in
 662 the six aerosol samples were calculated and listed as C_{18.7}H_{23.5}O_{6.99}N_{0.73}S_{0.09},
 663 C_{19.9}H_{21.5}O_{7.65}N_{0.34}S_{0.03}, C_{16.1}H_{13.3}O_{5.37}N_{0.68}S_{0.23}, C_{15.2}H_{13.7}O_{4.24}N_{0.45}S_{0.41},
 664 C_{13.4}H_{18.0}O_{7.52}N_{0.45}S_{0.40}, and C_{17.3}H_{21.1}O_{5.65}N_{0.53}S_{0.08}. The BB aerosols had higher

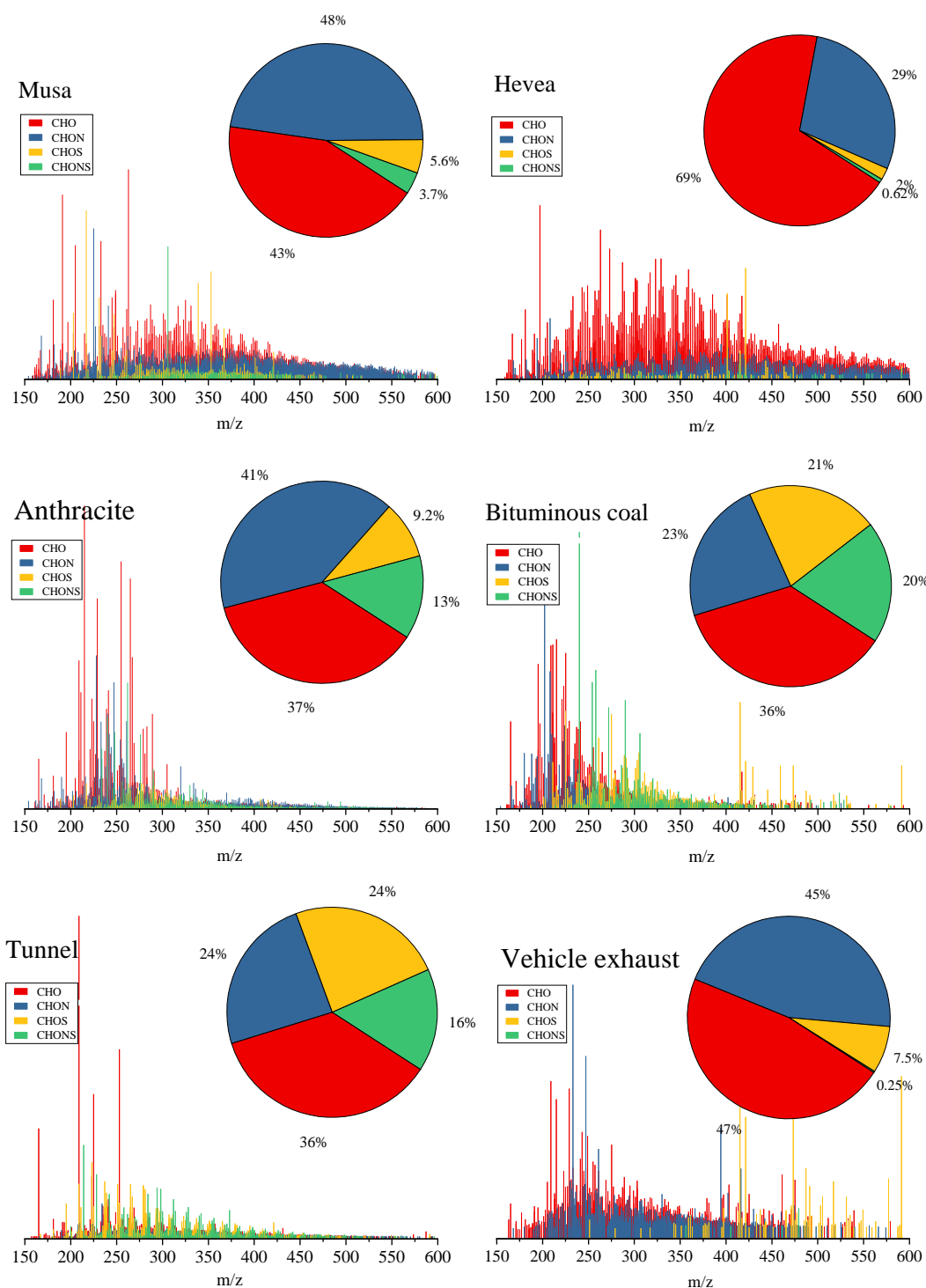
665 contents of C and H, while the CC aerosols and tunnel aerosol had higher contents of
 666 S.
 667 **Table 2.** Number of formulae in each compound category and the average values of elemental
 668 ratios, molecular weight (MW), double-bond equivalents (DBE), and aromaticity index (AI_{mod}) in
 669 the WSOC from the three origins.

<u>Samples</u>	<u>Elemental composition</u>	<u>Number of formulae</u>	<u>MW_w</u>	<u>DBE_w</u>	<u>AI_{mod,w}</u>	<u>O/C_w</u>	<u>H/C_w</u>	<u>DBE/C_w</u>
<u>Musa</u>	<u>Total</u>	<u>4534</u>	<u>372.55</u>	<u>8.36</u>	<u>0.33</u>	<u>0.37</u>	<u>1.25</u>	<u>0.45</u>
	<u>CHO</u>	<u>1504</u>	<u>367.73</u>	<u>8.08</u>	<u>0.32</u>	<u>0.38</u>	<u>1.25</u>	<u>0.43</u>
	<u>CHON</u>	<u>2375</u>	<u>384.06</u>	<u>9.31</u>	<u>0.39</u>	<u>0.34</u>	<u>1.22</u>	<u>0.48</u>
	<u>CHOS</u>	<u>329</u>	<u>320.06</u>	<u>4.59</u>	<u>0.15</u>	<u>0.51</u>	<u>1.46</u>	<u>0.34</u>
	<u>CHONS</u>	<u>323</u>	<u>358.24</u>	<u>5.04</u>	<u>0.12</u>	<u>0.51</u>	<u>1.51</u>	<u>0.35</u>
<u>Hevea</u>	<u>Total</u>	<u>3174</u>	<u>387.05</u>	<u>10.32</u>	<u>0.42</u>	<u>0.38</u>	<u>1.08</u>	<u>0.52</u>
	<u>CHO</u>	<u>1610</u>	<u>377.86</u>	<u>10.06</u>	<u>0.42</u>	<u>0.38</u>	<u>1.08</u>	<u>0.51</u>
	<u>CHON</u>	<u>1408</u>	<u>409.40</u>	<u>11.29</u>	<u>0.46</u>	<u>0.39</u>	<u>1.05</u>	<u>0.55</u>
	<u>CHOS</u>	<u>108</u>	<u>376.68</u>	<u>7.00</u>	<u>0.23</u>	<u>0.38</u>	<u>1.32</u>	<u>0.39</u>
	<u>CHONS</u>	<u>48</u>	<u>410.33</u>	<u>5.08</u>	<u>0.09</u>	<u>0.47</u>	<u>1.60</u>	<u>0.30</u>
<u>Anthracite</u>	<u>Total</u>	<u>3930</u>	<u>308.65</u>	<u>10.82</u>	<u>0.65</u>	<u>0.33</u>	<u>0.83</u>	<u>0.67</u>
	<u>CHO</u>	<u>990</u>	<u>283.07</u>	<u>11.06</u>	<u>0.67</u>	<u>0.28</u>	<u>0.77</u>	<u>0.67</u>
	<u>CHON</u>	<u>1808</u>	<u>323.71</u>	<u>11.67</u>	<u>0.71</u>	<u>0.34</u>	<u>0.81</u>	<u>0.69</u>
	<u>CHOS</u>	<u>464</u>	<u>308.97</u>	<u>8.73</u>	<u>0.49</u>	<u>0.36</u>	<u>0.95</u>	<u>0.59</u>
	<u>CHONS</u>	<u>668</u>	<u>332.83</u>	<u>8.99</u>	<u>0.52</u>	<u>0.46</u>	<u>0.95</u>	<u>0.63</u>
<u>Bituminous coal</u>	<u>Total</u>	<u>1375</u>	<u>282.91</u>	<u>9.63</u>	<u>0.61</u>	<u>0.28</u>	<u>0.90</u>	<u>0.63</u>
	<u>CHO</u>	<u>399</u>	<u>259.21</u>	<u>10.40</u>	<u>0.66</u>	<u>0.22</u>	<u>0.82</u>	<u>0.65</u>
	<u>CHON</u>	<u>411</u>	<u>267.68</u>	<u>9.92</u>	<u>0.69</u>	<u>0.27</u>	<u>0.86</u>	<u>0.67</u>
	<u>CHOS</u>	<u>302</u>	<u>324.65</u>	<u>9.51</u>	<u>0.49</u>	<u>0.28</u>	<u>0.99</u>	<u>0.57</u>
	<u>CHONS</u>	<u>263</u>	<u>299.28</u>	<u>7.98</u>	<u>0.56</u>	<u>0.43</u>	<u>0.98</u>	<u>0.63</u>
<u>Tunnel</u>	<u>Total</u>	<u>2746</u>	<u>317.68</u>	<u>5.68</u>	<u>0.35</u>	<u>0.56</u>	<u>1.34</u>	<u>0.42</u>
	<u>CHO</u>	<u>803</u>	<u>298.29</u>	<u>7.69</u>	<u>0.49</u>	<u>0.50</u>	<u>1.06</u>	<u>0.54</u>

	<u>CHON</u>	<u>1049</u>	<u>340.18</u>	<u>7.50</u>	<u>0.38</u>	<u>0.51</u>	<u>1.22</u>	<u>0.49</u>
	<u>CHOS</u>	<u>508</u>	<u>310.74</u>	<u>2.73</u>	<u>0.03</u>	<u>0.59</u>	<u>1.71</u>	<u>0.23</u>
	<u>CHONS</u>	<u>386</u>	<u>337.90</u>	<u>2.78</u>	<u>0.46</u>	<u>0.81</u>	<u>1.77</u>	<u>0.25</u>
	<u>Total</u>	<u>1301</u>	<u>327.71</u>	<u>7.96</u>	<u>0.41</u>	<u>0.33</u>	<u>1.22</u>	<u>0.46</u>
<u>Vehicle</u>	<u>CHO</u>	<u>561</u>	<u>311.62</u>	<u>8.02</u>	<u>0.43</u>	<u>0.30</u>	<u>1.19</u>	<u>0.46</u>
<u>exhaust</u>	<u>CHON</u>	<u>673</u>	<u>320.62</u>	<u>7.28</u>	<u>0.41</u>	<u>0.40</u>	<u>1.27</u>	<u>0.47</u>
	<u>CHOS</u>	<u>63</u>	<u>467.88</u>	<u>11.88</u>	<u>0.36</u>	<u>0.19</u>	<u>1.19</u>	<u>0.44</u>
	<u>CHONS</u>	<u>4</u>	<u>438.78</u>	<u>2.21</u>	<u>0</u>	<u>0.46</u>	<u>1.97</u>	<u>0.12</u>

670 In this study, these identified molecular formulas were classified into four main
671 compound groups based on their compositions: CHO, CHON, CHOS, and CHONS.
672 CHO compounds refer to the compounds that contained carbon, hydrogen, oxygen,
673 and the other compound groups that were defined analogously. The relative
674 abundances of the four compound groups were calculated by the magnitude of each
675 peak divided by the sum of magnitudes of all identified peaks and showed in Figure 4.
676 CHO was the most abundant component in the WSOC, accounting for 43% - 69% of
677 total intensities of BB aerosols, 36% - 37% of CC aerosols, and 36% - 47% of vehicle
678 emissions, respectively. CHO in the BB and CC aerosols were lower than those of
679 mass spectra from simulated combustion experiments (BB (53%-72%) and CC (43%))
680 (Song et al., 2018). Generally, CHO formulas were consistent with species reported
681 previously as lignin-pyrolysis products (Fleming et al., 2017), and they detected this
682 fraction was 43.1% ± 14.6% in brushwood-chulha cook firers. CHON was abundant
683 in the three sources. This result was different from the findings that CHON species
684 had a higher percentage in BB smoke and were not abundant in CC smoke (Song et al.,
685 2018). The high fraction of CHON in the CC aerosols could be due to that the
686 N-containing compounds in the BB smoke PM_{2.5} come from the nitrogen content in
687 the fuels (Coggon et al., 2016), and the contents in coal fuels were comparable to
688 biomass fuels (See Table S1 and S2). However, S-containing compounds were more
689 abundant in the CC aerosols (9.0%-21% for CHOS and 13%-20% for CHONS,
690 respectively) and tunnel aerosol (24% for CHOS and 16% for CHONS, respectively)

691 than those in the BB aerosols (2.0%-5.6% for CHOS and 0.62%-3.7% for CHONS,
692 respectively) and vehicle exhaust particle (7.5% for CHOS and 0.25% for CHONS,
693 respectively), consistent with the previous studies (Song et al., 2018;Wang et al.,
694 2017). ESI was more efficient in ionizing S-containing compounds and most of them
695 were selectively ionized by ESI-, suggesting that they were polar species such as
696 organosulfates (Lin et al., 2018). Our study reported that S-containing compounds in
697 the WSOC were associated with CC emissions by combining with ¹⁴C data (Mo et al.,
698 2018). Furthermore, the relative abundances of group species in the CC aerosols and
699 TA were similar to those of water extracts in the hazy day (Jiang et al., 2016),
700 indicating both sources could be the important contributors of haze. However,
701 differences between tunnel aerosol and vehicle exhaust particle were observed,
702 indicating S-containing compounds in the tunnel aerosol were more secondary
703 formation.



704

705 **Figure 4.** Negative ESI FT-ICR mass spectra of WSOC in the six aerosol samples. Different
 706 formula groups were color-coded. The six pie charts showed the relative intensities of different
 707 formula groups.

708 Van Krevelen (VK) diagram is a useful tool that provides a visual graphic display
 709 of compound distribution, and to some extent, use to qualitatively identify different
 710 composition domains in organic mixtures (Song et al., 2018;Lv et al., 2016;Smith et

711 al., 2009). In this study, each source showed similar VK patterns. Musa and Hevea
712 burning had a resemble VK diagram to that of WSOC in straw burning and fog water
713 (Schmitt-Kopplin et al., 2010;Mazzoleni et al., 2010). S-containing compounds in
714 tunnel aerosol with high O/C and H/C ration were similar to the aerosol-derived
715 WSOC in New York and Virginia (Wozniak et al., 2008). Six dominate domains were
716 identified in the WSOC, including lignins, carbohydrates, tannins, proteins,
717 condensed aromatic, and unsaturated hydrocarbons. As shown in Figure S9, results
718 showed compounds observed in the CC aerosols had lower H/C and O/C ratios than
719 those in the BB aerosols and vehicle emissions, indicating a higher unsaturated degree
720 and lower oxidation level. There were compounds outside the specified regions,
721 which had a high H/C ratio (≥ 2.2), and DBE = 0 correspond to saturated oxygenated
722 species and could be some long-chain polyalcohols (Lin et al., 2012a).

723 The mass spectra of MSOC exhibited differences from WSOC (Figure S10),
724 especially in the BB aerosols and vehicle emissions that exhibited larger m/z in the
725 range of 350-600. The detected formulas in the MSOC were much lower than those in
726 the WSOC, with the number of 4502, 3628, and 1069 for the BB, CC, and vehicle
727 emission aerosols, respectively. The reason could be due to that ESI can efficiently
728 ionize the polar compounds, and the methional extracts after water-extracted may
729 contain more moderate- and low- polar compounds that were not easily ionized. The
730 average molecular formulas were $C_{26.9}H_{46.2}O_{4.27}N_{0.24}S_{0.02}$, $C_{23.3}H_{34.9}O_{5.18}N_{0.20}S_{0.02}$,
731 $C_{18.2}H_{19.2}O_{4.24}N_{0.92}S_{0.03}$, $C_{22.4}H_{20.7}O_{3.01}N_{0.38}S_{0.05}$, $C_{22.6}H_{44.1}O_{5.70}N_{0.74}S_{0.11}$, and
732 $C_{25.2}H_{48.5}O_{4.86}N_{0.58}S_{0.08}$ of MSOC in the six aerosol samples, respectively, showing
733 higher C and H contents than their corresponding formulas of WSOC but a decreasing
734 trend in the O contents.

735 CHO and CHON were the main components in the MSOC, accounting for about
736 90% of the total intensities (CHO plus CHON). CHO was the most abundant category
737 observed in the BB aerosols (78%-80%). The elemental compositions observed in CC
738 aerosols were different between bituminous coal and anthracite combustion, where the
739 latter had more abundance of CHON (73%), but the former with more CHO (60%),
740 which was consistent with their corresponding WSOC and could be due to anthracite

741 had higher N content but lower O content than bituminous coal (see Table S2).
742 However, CHON in the BB aerosols (18%-20%) exhibited lower abundance than
743 those in the CC aerosols and vehicle emissions. These results provided a new sight for
744 those CHON compounds that contributed to a high abundance in fossil fuel
745 combustion in the MSOC. Besides, S-containing compounds were not abundant in the
746 MSOC. It is potential to due to that S element combined with O atom may exhibit
747 higher polarity.

748 Figure S11 showed the VK diagram of MSOC in the six aerosol samples. More
749 formulas in BB aerosols exhibited two distinct groups with H/C 1.4-2.2 and 0.6-1.4 vs.
750 O/C 0.1-0.5, inside three domains (lignins, proteins, and lipids). Compounds in CC
751 aerosols with lower H/C and O/C ratios were dominant in the domains of lignins and
752 condensed aromatic, especially in the bituminous CC aerosol with more unsaturated
753 hydrocarbon. Tunnel aerosol showed a wide range of O/C in S-containing compounds
754 and a wide range of H/C in non-S-containing compounds. In contrast, compounds in
755 vehicle exhaust particle had a wide range of H/C but a narrow O/C ratio. The VK
756 diagram with fewer S-containing compounds in the vehicle exhaust particle showed a
757 similar characteristic to the distribution of non-S-containing compounds in tunnel
758 aerosol, indicating the difference was mainly due to the S-containing compounds.

759 Table 2 and S5 presented the relative abundance weighted molecular weight
760 (MW_w), Double bonds equivalence (DBE_w), and modified aromaticity index ($AI_{mod,w}$)
761 of WSOC and MSOC, respectively (see SI). DBE_w was used as a measure of
762 unsaturated level in a moleculer, and $AI_{mod,w}$ could be used to estimate the fraction of
763 aromatic and condensed aromatic structures (Song et al., 2018;Lv et al., 2016;Koch
764 and Dittmar, 2006). BB aerosols had higher MW_w values than CC and vehicle
765 emissions in the WSOC. Besides, higher DBE_w and $AI_{mod,w}$ values were observed in
766 the CC aerosols than the other two sources. MSOC had higher MW_w but lower AI_{mod}
767 values (except for CC aerosols) than the corresponding WSOC. Furthermore, CHO
768 and CHON compounds had higher DBE_w and $AI_{mod,w}$ values than S-containing
769 substances, consistent with the earlier results (Lin et al., 2012b;Lin et al., 2012a).

770 Figure S12 showed the fraction of AI_{mod} values of WSOC in the six aerosol
771 samples, where the formulas were classified according to their AI_{mod} (aliphatic ($AI =$
772 0), olefinic ($0 < AI \leq 0.5$) and aromatic ($AI > 0.5$)). The results illustrated that the
773 fraction of aromatic structure in non-S-containing compounds was higher than those
774 in S-containing compounds. CC aerosols had a higher aromatic fraction than BB
775 aerosols and vehicle emissions, especially in CHO and CHON (up to 89% of total ion
776 intensities). In the BB aerosols, the non-S-containing compounds had a high fraction
777 of olefinic structure, following by aromatic structure, but the S-containing compounds
778 had a higher aliphatic and olefinic structure than aromatic structure. Besides, a higher
779 fraction of aliphatic in vehicle emissions was observed in S-containing compounds
780 (especially in tunnel aerosol (exceed 81%)). These aliphatic S-containing compounds
781 might form by the precursors (long-chain alkanes) from vehicle emissions (Tao et al.,
782 2014), which had higher H/C and lower DBE values (see Table 2). However, the
783 previous study showed that AI must be regarded as the most conservation approach
784 and may result in an underestimate of the aromatic structures (Koch and Dittmar,
785 2006), which was observed in Beijing aerosols (Mo et al., 2018). Although AI_{mod}
786 identified more compounds as aromatic and condensed aromatic components than AI,
787 the AI_{mod} may introduce uncertainties for individual molecules, which was
788 demonstrated by Koch and co-author.

789 Consistent with WSOC, high fractions of the aromatic structure were observed in
790 non-S-containing compounds than S-containing compounds, and higher fractions of
791 aromatic structure in the CC aerosols were observed than BB aerosols and vehicle
792 emissions in the MSOC (Figure S13). Furthermore, we found that the fraction of
793 aliphatic in MSOC was higher than that in WSOC, indicating more fat-like
794 compounds.

795 *Different chemical characteristic of BB, CC, and vehicle emissions*

796 Figure S14 plotted the Venn diagram of formulas in the WSOC fraction in the six
797 aerosol samples for determining the unique elementals in the mass spectra. The

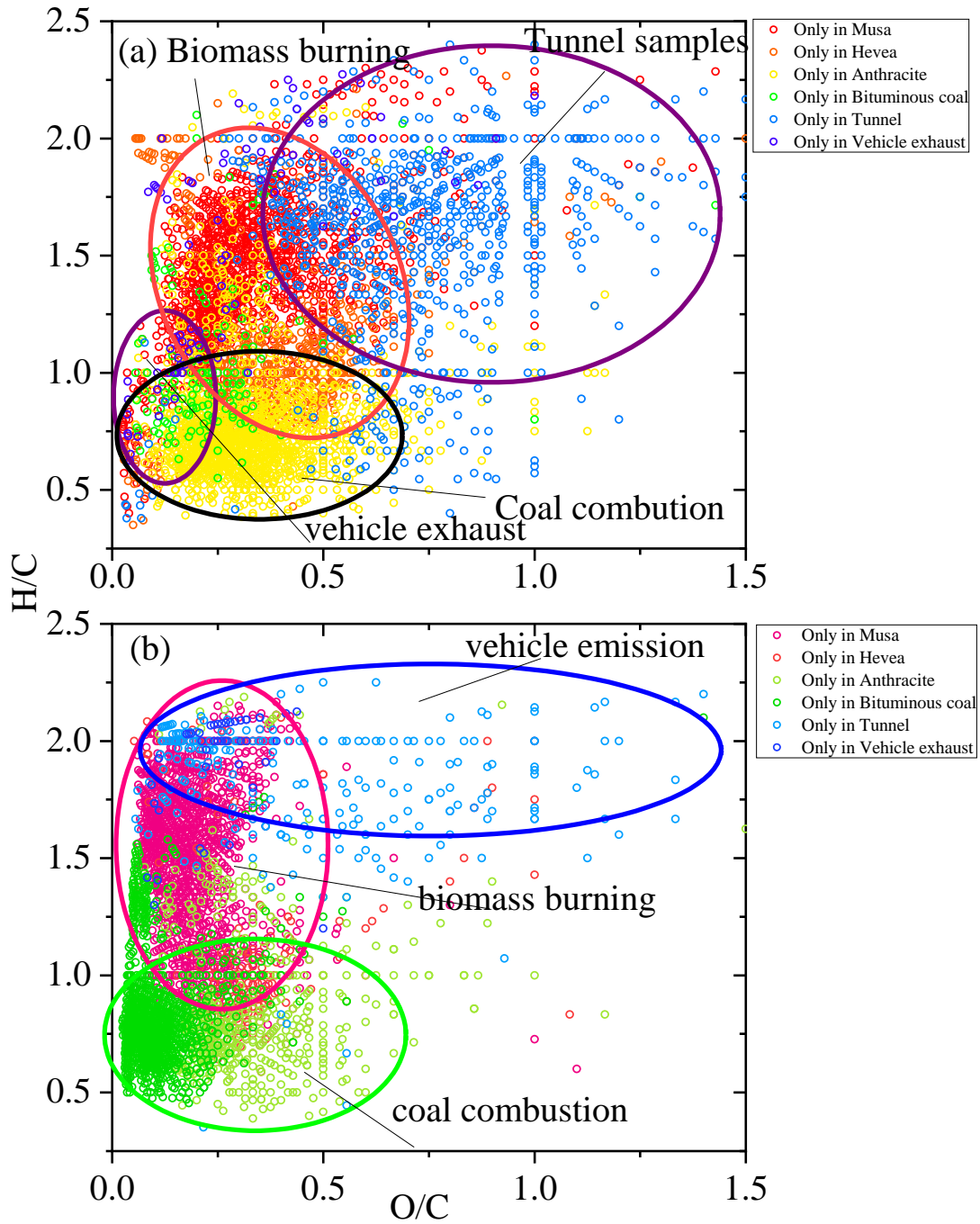
798 previous study identified the unique elementals of water-soluble HULIS in simulated
799 BB and CC smokes, which presented different molecular characteristics between
800 biomasses, as well as between biomass and coal (Song et al., 2018). In this study, we
801 combined more formulas of different sources to determine the unique molecular and
802 more limitation was set, which would provide more identified characteristics for each
803 source. 212 molecular formulas were detected simultaneously in the six aerosol
804 samples, suggesting the compounds could be more detected in the atmosphere. It is
805 noting that without any further information, it is not possible to decide whether these
806 common formulas represent the same compounds. There were 112 of CHO unique
807 molecular in 212 and 98 of CHON but only 2 of CHOS molecular. CHO compounds
808 were relatively small aromatic compounds with 8-10 C atoms and 3-8 O atoms and
809 DBE 5-13 and multiple acidic polar functional groups (Figure S15). It is noting that
810 lines in Figure S15 indicate DBE reference values of linear conjugated polyenes
811 C_xH_{x+2} with $DBE=0.5 \times C$, and fullerene-like hydrocarbons with $DBE=0.9 \times C$, where
812 the data points inside this region are potential BrC chromophores (Lin et al., 2018).
813 For example, organic acids ($C_8H_6O_5$ ($DBE=6$) was detected in Urban $PM_{2.5}$ (Yassine
814 et al., 2012), as well as $C_9H_8O_5$ (6), $C_{14}H_{14}O_4$ (8), $C_{13}H_{14}O_5$ (7), which allowed them
815 to ionization in the ESI- mode and were identified as potential BrC chromophores. In
816 total, all of CHON compounds had $O/N \geq 2$ (5.3 ± 1.28 , 2.5-7) (Figure S15), allowing
817 for the assignment of at least one nitro ($-NO_2$) or nitrooxy ($-ONO_2$) group and other
818 oxygen-containing groups (i.e., $-OH$ and $-COOH$). Except for $C_{19}H_{41}O_7N$ ($DBE=0$),
819 the remaining compounds with $DBE \geq 5$ were suggested as nitro-aromatic and
820 nitrophenol derivatives (Mo et al., 2018; Lin et al., 2018). CHOS species only had two
821 formulae including $C_{18}H_{38}O_7S$ (0) and $C_{20}H_{38}O_7S$ (2). It was reported that O_7S groups
822 were the most abundant species class in CHOS identified in water extracts of $PM_{2.5}$
823 (Jiang et al., 2016).

824 There were more observed unique peaks of WSOC in the BB aerosols (total 1947)
825 compared to CC aerosols (1583) and vehicle emissions (813). However, only 143 and
826 83 molecular were identified in bituminous CC and vehicle exhaust particle,

827 respectively. Among the observed compounds, 1353 and 1440 unique molecular
828 formulas were detected in in combustion of Musa and anthracite, respectively,
829 showing a significant difference from the others. Figure 5 (a) showed the VK diagram
830 of these unique formulas of WSOC for each sample, where four regions were circled
831 for representing different sources. The results indicated that these unique compounds
832 in different sources had a distinctive chemical characteristic. That may be the reason
833 that resulted in variable fluorescent spectra in different sources (discussed above).
834 Additionally, the diagram showed that the unique molecular in CC aerosols located in
835 the region with lower H/C and O/C, and vehicle emissions between tunnel aerosol and
836 vehicle exhaust particle located in two distinct regions.

837 Figure 6 showed plots of the DBE vs. the number of carbon atoms in the unique
838 molecular formulas of all aerosol samples. These compounds observed in the BB
839 aerosols were largely CHO and CHON (CHO and CHON, 88% - 93%) with C
840 numbers ranging from 6 to 40 and DBE ranging from 0 to 31, with no regular
841 distribution. S-containing compounds were the important components in the unique
842 molecular formulas of CC aerosols (CHOS and CHONS, 38%-75%) and vehicle
843 emissions (CHOS and CHONS, 41%-66%). However, only 7%-12% of the total
844 unique molecular formulas were observed in BB aerosols. As shown in Figure 6, the
845 region marked by blue box denoted the high intensities of compounds in unique
846 formulas of each sample. The high-intensity compounds detected in the Musa burning
847 aerosol were mainly C number from 14 to 24, DBE from 7 to 13, and two N atoms,
848 such as $C_{20}H_{26}O_7N_2$ (9), $C_{18}H_{24}O_2N_2$ (8), $C_{22}H_{28}O_6N_2$ (10), $C_{19}H_{26}O_7N_2$ (8),
849 $C_{21}H_{28}O_6N_2$ (7), $C_{14}H_{18}O_7N_2$ (7), $C_{24}H_{30}O_8N_2$ (11), and $C_{21}H_{24}O_5N_2$ (11) and so on.
850 Instead of Musa, the abundant compounds in the Hevea were mainly $C_{24}H_{22}O_9$ (14),
851 $C_{28}H_{28}O_{11}$ (15), and $C_{28}H_{26}O_{11}$ (16), and so on. Although the difference between
852 burning of Musa and Hevea appeared, the VK diagram (Figure 5) did not show
853 distinct changes. The high-intensity compounds in the anthracite combustion with
854 lower C atoms than in the bituminous CC, which were main $C_{14}H_8O_5N_2$ (12),
855 $C_{12}H_{11}O_4NS$ (8), $C_{12}H_{10}O_8N_2$ (9), while in bituminous CC were main $C_{28}H_{28}O_4S$ (15)
856 and its homolog of $C_{27}H_{26}O_4S$ (15), and $C_{19}H_{16}O_3S$ (12). The abundant compounds in

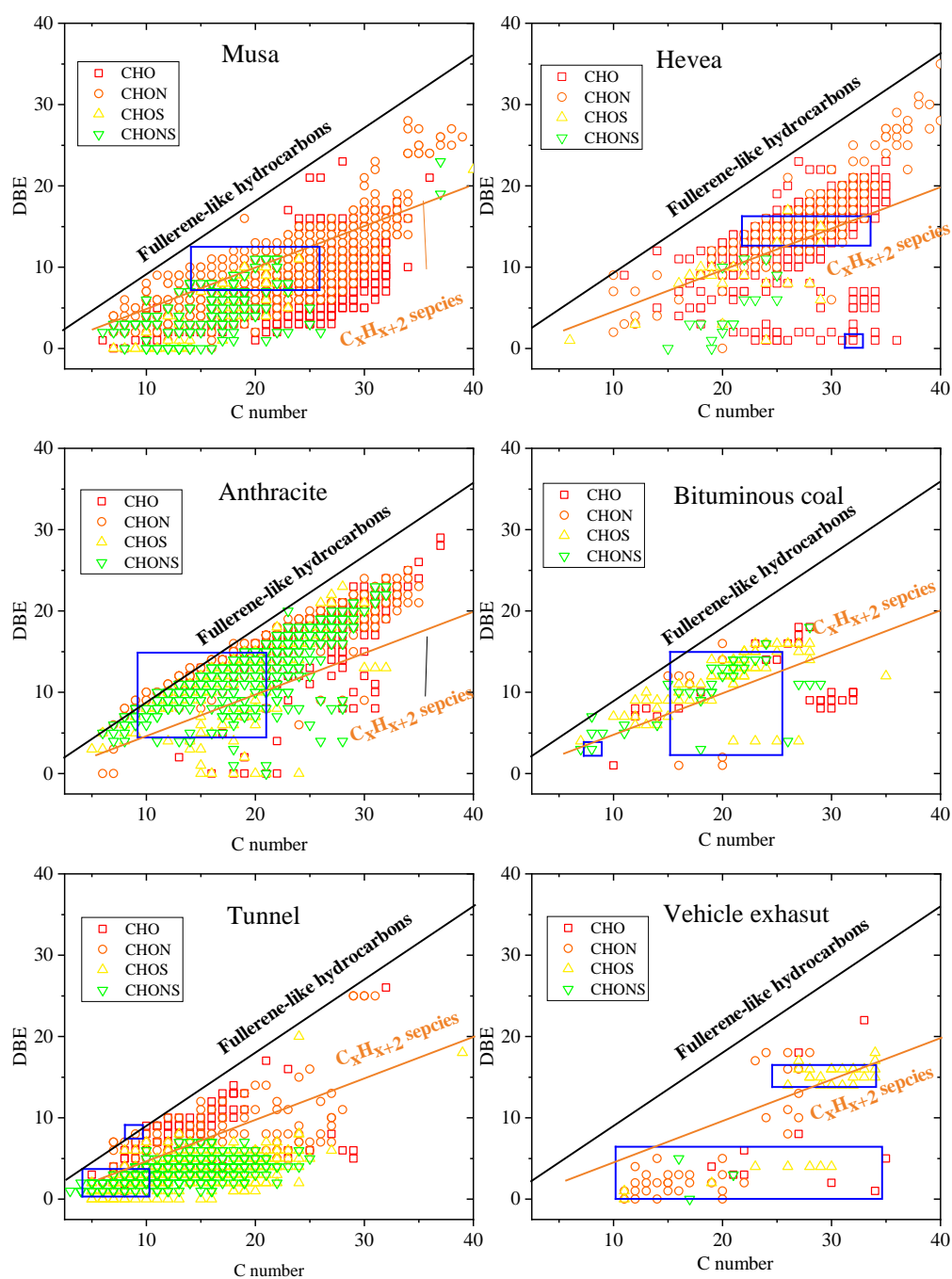
857 tunnel aerosol had a lower unsaturation degree, such as C₄H₉O₇NS (1), C₅H₁₁O₇NS
858 (1), C₇H₁₃O₅S (1). In the vehicle exhaust particle, the high intensity of compounds
859 was one fraction with low C atoms and DBE (C₂₁H₄₀O₈N₂S (3), C₂₆H₄₆O₃S (4)), and
860 the other fraction with high C atoms and DBE (C₃₂H₃₄O₈S (16), C₃₀H₃₄O₅S (14)).
861 These findings are essential because these unique molecular formulas in different
862 sources may have specific chemical composition, which would help the source
863 apportionment of aerosols.



864

865 Figure 5. A Van Krevelen diagram of WSOC (a) and MSOC (b) in the six samples.

866 Different color indicates unique formulas detected in each sample.



867

868 Figure 6. DBE vs. C number for unique molecular compounds of WSOC for the six aerosol
 869 samples. Lines indicate DBE reference values of linear conjugated polyenes C_xH_{x+2} with
 870 $DBE=0.5 \times C$, and fullerene-like hydrocarbons with $DBE=0.9 \times C$. The regions marked by blue box
 871 denoted the high intensities of compounds.

872 Comparison with WSOC, Figure S16 showed fewer compounds in common in
 873 the MSOC for the six aerosol samples. There were only 44 compounds common in the

874 six aerosol samples. A total of 26 and 14 of the 44 formulas were CHO and CHON,
875 respectively, but only 4 of the 44 formulas were S-containing compounds. As shown
876 in Figure S17, there were only three compounds (C₁₇H₈O₂ (13), C₁₈H₁₄O (12),
877 C₁₈H₁₂O₂ (13)) in CHO group, and one compound (C₁₄H₁₁O₄N (10)) in CHON group
878 inside the potential BrC region. The remaining compounds had a high C number
879 (18-35), low O atoms (1-7), and low DBE (0-2), suggesting that they mostly had fatty
880 acid structures.

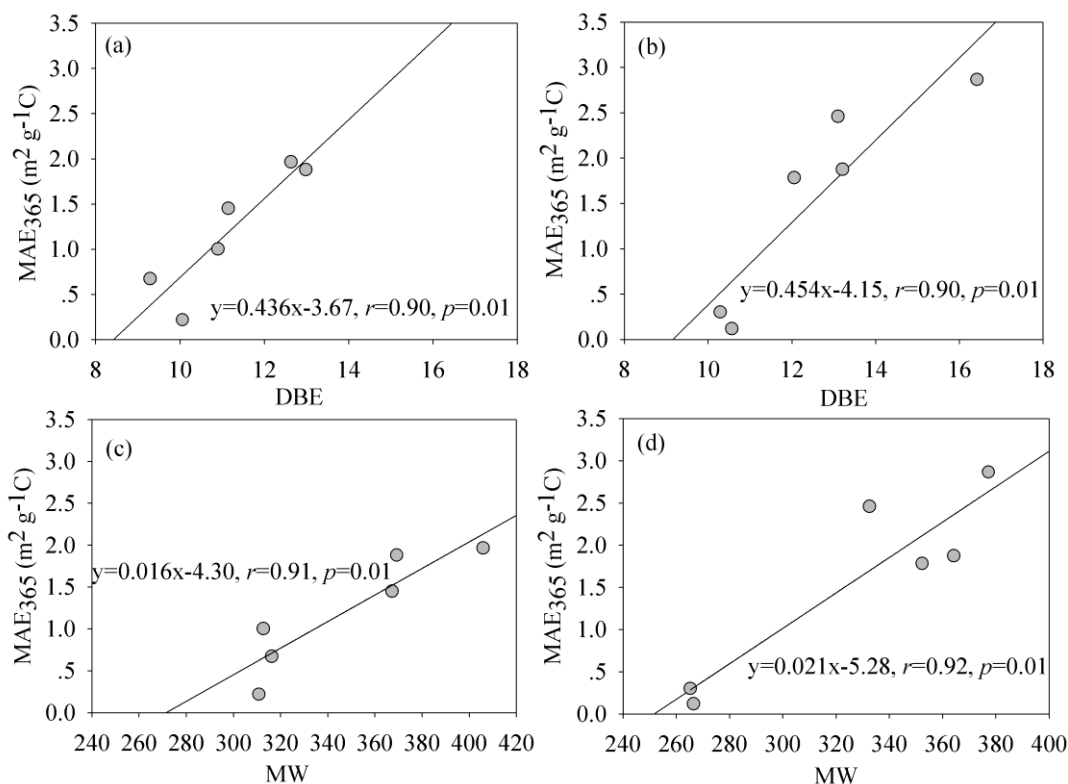
881 These unique molecular in VK also showed similar results comparing to WSOC
882 (Figure 5 (b)), further confirming the special characters in different sources. Expect
883 for tunnel aerosol (about 50%), these unique formulas in the BB aerosols, CC aerosols,
884 and vehicle exhaust particle was dominant by CHO- and CHON-groups (Figure S18),
885 indicating S-containing compounds with lower polarity could be originated from the
886 secondary formation of vehicle exhaust. The high-intensity compounds were
887 C₃₅H₆₉O₅N (2), C₃₈H₇₆O₄ (1) for Musa burning; C₂₆H₂₂O₇ (16), C₂₈H₂₆O₇ (16) for
888 Hevea burning; C₁₄H₁₂O₆N₂ (10), C₁₇H₁₄O₅N₂ (12) for anthracite combustion;
889 C₂₃H₁₆O (16), C₂₄H₁₈O (16), C₂₄H₁₄O (18) for bituminous CC;
890 C₄H₉O₇NS(1), C₂₄H₄₂O₃S (4), C₈H₁₆O₅S (1) for tunnel aerosol, and C₂₆H₃₇O₅NS(7),
891 C₂₂H₄₆O₇(0) for vehicle exhaust particle, respectively.

892 **3.4 Link of molecular composition and optical properties**

893 In the above statements, we discussed the light absorption and fluorescence properties
894 from aerosols in the three different sources. The light absorption capacity of WSOC
895 and MSOC was essential to assess the evolution of BrC, and fluorescence spectra
896 were sensitive to different sources and could help for the source apportionment of BrC.
897 Besides, we evaluated the molecular composition of the three sources. Therefore,
898 understanding the factors affecting the optical properties of BrC is important. It was
899 reported that the MAE in the BB experiments depended largely on burning conditions
900 (Chen and Bond, 2010) and in the CC experiments depended on coal maturity (Li et
901 al., 2018). Chen et al., (2017b) illustrated that higher light absorption capacity were

902 associated with low- and medium-polar fractions that contained aromatic and polar
903 functional groups (O or both O and N atoms). Sources play an important role in light
904 absorption capacity, consistent with our current study. The MAE₃₆₅ values of WSOC
905 in highly BB-impacted areas were two times higher than in low BB-impacted areas in
906 the Southeastern United States (Hecobian et al., 2010). Atmospheric aging has a
907 significant effect on the light absorption capacity of BrC (Li et al., 2019), but the
908 mechanism involved is very complex. The response of the light absorption capacity of
909 different types of BrC to aging is highly variable, and enhancement or reduction in the
910 light absorption capacity of BrC is possible (Li et al., 2019). These results indicated
911 that light absorption capacity might be affected by various factors. In this study,
912 higher MAE₃₆₅ values were observed in the BB and CC aerosols than vehicle
913 emissions, and the chemical structures and unsaturation degree of different sources
914 were discussed. Next, we further discussed the relationships between optical
915 properties and chemical structures.

916 In order to reduce the influence of non-absorbing substances, we firstly determined
917 these compounds, which were potential to absorb light radiation based on the above
918 statement. Mo et al., (2018) reported that MAE₃₆₅ of HULIS in aerosols was affected
919 by oxidation level and unsaturation degree. In this study, the MAE₃₆₅ had no
920 significant correlation with O/C, indicating that light absorption capacity does not
921 appear to be affected by their oxidized properties in the source aerosols. Instead of
922 O/C, the MAE₃₆₅ had a well positive correlation with the average DBE and MW,
923 respectively (Figure 7), suggesting the unsaturation level and MW played a vital role
924 in the light absorption capacity of source samples. Field experiments indicated that the
925 majority of absorption was the larger molecules (>500 Da) (Di Lorenzo et al., 2017).
926 It is crucial to knowledge the relationship between light absorption of source samples
927 and their chemical structures due to the compounds in fresh emissions that may
928 undergo a secondary process and introduce more uncertainty for their optical
929 properties.



930

931 Figure 7. Relationship between DBE and MW of the potential BrC molecules and the
 932 MAE₃₆₅ of WSOC (a, c) and MSOC (b, d) in the six samples, respectively.

933 Fluorescence spectra could provide more information than UV-vis spectra. A red
 934 shift in the excitation/emission maximum could indicate increased aromaticity and
 935 higher molecular weight (Ghidotti et al., 2017). Field observation had demonstrated
 936 that chromophore components were associated with chemical structures (Chen et al.,
 937 2016b;Chen et al., 2016a;Stubbins et al., 2014). Chen et al., (2016b) illustrated that
 938 the fluorescent components of HULIS-1 and HULIS-2 were correlated positively with
 939 CO⁺ and CO₂⁺, and C_xH_y⁺ and C_xH_yO₁⁺ groups ions, respectively, using the
 940 correlation analysis of the relative intensities of ion groups in the high-resolution
 941 aerosol mass spectrometers (HR-AMSs) and relative contents of fluorescence
 942 components. In another study, Chen et al., (2016a) demonstrated that fluorescent
 943 components had strong links with chemical groups in the Fourier transform infrared
 944 (FT-IR) spectra, including the oxygenated functional groups (nonacidic carbonyl C=O
 945 and carboxylic COOH groups), aliphatic C-H group, amine C-NH₂, and alcohol

946 C-OH groups. The chromophores are sensitive to sources, and it is very important to
947 understand the molecular composition of chromophores for classification and source
948 apportionment of atmospheric BrC. However, the ESI- cannot ionize the most typical
949 BrC chromophores such as O-heterocyclic PAHs (O-PAHs), N-heterocyclic PAHs
950 (O-PAHs) (Lin et al., 2018), which was not enough to discuss the relationship between
951 the fluorescence spectra and molecular composition. The combination of atmospheric
952 pressure photoionization (APPI+ and APPI -) and ESI (+ and -) may provide more
953 ionized compounds, but these techniques were not with the scope of our study.

954 **4 Conclusions**

955 We conducted comprehensive measurements on light absorption, fluorescence, and
956 molecular compositions of dissolved BrC derived from smoke particles during the
957 simulated combustion of biomass and coal, as well as vehicle emissions. We observed
958 ~~the~~ BB and CC aerosols had high MAE₃₆₅ values than vehicle emissions, on average,
959 1.6 ± 0.55, 1.3 ± 0.34, 2.0 ± 0.75, and 0.71 ± 0.30 m² g⁻¹ C for BB, anthracite
960 combustion, bituminous CC and vehicle emission aerosols, respectively. In addition,
961 BrC emitted from BB (2.3 ± 1.1 m² g⁻¹ C) and bituminous CC (3.2 ± 1.1 m² g⁻¹ C) in
962 the MSOC exhibited stronger light absorption capacity than those in the WSOC, but
963 opposite results were found in anthracite combustion aerosols (0.88 ± 0.74 m² g⁻¹ C)
964 and vehicle emissions (0.26 ± 0.09 m² g⁻¹ C). ~~optical properties of the WSOC and~~
965 MSOC fractions and observed that the light absorption of methanol soluble BrC was
966 stronger. ~~EEM combining with PARAFAC analysis determined six six types of~~
967 fluorescent components that were assigned as two HULIS-1 (P1, and P6), three
968 PLOM (P2, P3, P5), and one undefinition (P4) in the WSOC in the source
969 samples. ~~were resolved in the WSOC and MSOC fractions by PARAFAC analysis,~~
970 respectively. The relative intensities of the fluorescent components ~~of the WSOC and~~
971 MSOC fractions mainly depended on the different types of ~~smoke particle~~ sources,
972 For example, HULIS-1 was abundant in tunnel aerosols, P2 was more intense in BB
973 aerosols but not observed in vehicle emissions, P4 was intense in CC aerosols and
974 vehicle emissions, P5 was more abundant in the fresh vehicle exhaust particles;

975 although P3 was not abundant it was ubiquitous in all tested aerosols. Similar to
976 WSOC, six fluorescent components were identified in MSOC. Although the
977 methanol-soluble chromophores were poorly understood, different characteristics
978 were observed in different sources, which were derived from several origins,
979 suggesting that the fluorescent components varied from source to source. This result
980 may be useful for fluorescence-based methods, which play an important role in the
981 classification and source identification of BrC dissolved in the atmosphere.

982 ~~We also discussed the possible structures of these chromophores. Our results~~
983 ~~indicate that these fluorescent components were mainly affected by functional groups,~~
984 ~~especially functional groups containing N and S. In the case of the WSOC fraction, P1~~
985 ~~and P6 components were mainly associated with aromatic organosulfate compounds;~~
986 ~~the P4 and P5 components were mainly associated with nitrooxy OS compounds and~~
987 ~~sulfonates, respectively. However, we did not elucidate the structures of the P2 and P3~~
988 ~~components. In the case of the MSOC fraction, the C1 component was mainly related~~
989 ~~to organosulfate compounds; the C3 component was related to CHO_{>1} groups; the C2~~
990 ~~component was mainly correlated with esters; and the C5 component was related to~~
991 ~~sulfonates. The C6 component was correlated well with S-containing compounds. As~~
992 ~~with the P2 and P3 components, we know little about the structure of the C4~~
993 ~~component. Our findings provide insights into the chemical structures of water and~~
994 ~~methanol-soluble chromophores, and these results may be useful for further aerosol~~
995 ~~studies, for source apportionment of dissolved BrC based on EEM fluorescence.~~

996 FT-ICR mass spectra showed that the m/z of the mainly compounds with m/z
997 200-400 in the WSOC and MSOC were m/z 350-600 (except for CC aerosols),
998 respectively. CHO and CHON were the main components in the three origins, but
999 S-containing compounds were more abundant in CC and tunnel aerosols than BB
1000 aerosol and vehicle exhaust particles in the WSOC. Similarly, MSOC mainly also
1001 contained CHO and CHON species but fewer S-containing compounds. BB aerosols
1002 had higher CHO species in MSOC but showed lower CHON than CC aerosols and
1003 vehicle emissions. Ven diagram showed that CC aerosols had more unsaturation

1004 degree and low oxidation level than the other two sources. This finding was further
1005 confirmed by a higher fraction of aromatic in CC aerosols. Unique formulas
1006 determined by Venn diagram showed certain specific chemical characteristics in VK
1007 diagram. BB aerosols emitted unique formulas with more CHO and CHON
1008 (88%-93%), while CC aerosols and vehicle emissions contained more S-containing
1009 compounds (38%-75% and 41%-46%, respectively). The relationship between optical
1010 properties and chemical structures showed the light absorption capacity was positively
1011 associated with an unsaturation degree and MW in the source emissions. Our study
1012 illustrated the important roles of sources in light-absorbing BrC and molecular
1013 compositions and the EEM-based method is handy for classification and source
1014 apportionment of chromophores in atmospheric aerosols.

1015 *Data availability.* The data used in this study are available upon request; please
1016 contact Gan Zhang (Zhanggan@gig.ac.cn) and Jun Li (junli@gig.ac.cn)

1017 *Supplement.* The supplement related to this article is available.

1018 *Author contributions.* JT, GZ, JL, and YC designed the experiment. JT and MC
1019 carried out the measurements and analyzed the data. JT, TS, YH, and HJ organized
1020 and performed the samplings. JT (Jianhui Tang) and BJ supported the fluorescence
1021 and FT-ICR MS instrument. JT wrote the paper. JL, YM, JS, PP, and GZ reviewed
1022 and commented on the paper.

1023 *Competing interests.* The authors declare that they have no conflict of interest.

1024 *Acknowledgements.* This study was supported by the Natural Science Foundation of
1025 China (NSFC; Nos. 41430645 and 41773120), the National Key R&D Program of
1026 China (2017YFC0212000), and the International Partnership Program of Chinese
1027 Academy of Sciences (Grant No.132744KYSB20170002).

1028 **Reference:**

1029 ~~Alexander, L., Smith, J. S., and Julia, L.: Molecular characterization of nitrogen-containing~~
1030 ~~organic compounds in biomass burning aerosols using high-resolution mass spectrometry,~~
1031 ~~Environ. Sci. Technol., 43, 3764-3771, <https://doi.org/10.1021/es803456n>, 2009.~~

1032 Andersson, C. A., and Bro, R.: The N-way Toolbox for MATLAB, Chemom. Intell. Lab. Syst., 52,
1033 1-4, [https://doi.org/10.1016/s0169-7439\(00\)00071-x](https://doi.org/10.1016/s0169-7439(00)00071-x), 2000.

1034 Andrade-Eiroa, Á., Canle, M., and Cerdá, V.: Environmental Applications of Excitation-Emission
1035 Spectrofluorimetry: An In-Depth Review I, Appl. Spectrosc. Rev., 48, 1-49,
1036 <https://doi.org/10.1080/05704928.2012.692104>, 2013.

1037 Bahram, M., Bro, R., Stedmon, C., and Afkhami, A.: Handling of Rayleigh and Raman scatter for
1038 PARAFAC modeling of fluorescence data using interpolation, J. Chemom., 20, 99-105,
1039 <https://doi.org/10.1002/cem.978>, 2006.

1040 Bhattacharya, R., and Osburn, C. L.: Multivariate Analyses of Phytoplankton Pigment
1041 Fluorescence from a Freshwater River Network, Environ. Sci. Technol., 51, 6683-6690,
1042 <https://doi.org/10.1021/acs.est.6b05880>, 2017.

1043 ~~Budisulistiorini, S. H., Riva, M., Williams, M., Chen, J., Itoh, M., Surratt, J. D., and Kuwata, M.:~~
1044 ~~Light-Absorbing Brown Carbon Aerosol Constituents from Combustion of Indonesian Peat~~
1045 ~~and Biomass, Environ. Sci. Technol., 51, 4415-4423, <https://doi.org/10.1021/acs.est.7b00397>,~~
1046 ~~2017.~~

1047 ~~Blair, S. L., MacMillan, A. C., Drozd, G. T., Goldstein, A. H., Chu, R. K., Pasa-Tolic, L., Shaw, J.~~
1048 ~~B., Tolic, N., Lin, P., Laskin, J., Laskin, A., and Nizkorodov, S. A.: Molecular~~
1049 ~~Characterization of Organosulfur Compounds in Biodiesel and Diesel Fuel Secondary~~
1050 ~~Organic Aerosol, Environ. Sci. Technol., 51, 119-127,~~
1051 ~~<https://doi.org/10.1021/acs.est.6b03304>, 2017.~~

1052 Chen, H., Liao, Z. L., Gu, X. Y., Xie, J. Q., Li, H. Z., and Zhang, J.: Anthropogenic Influences of
1053 Paved Runoff and Sanitary Sewage on the Dissolved Organic Matter Quality of Wet Weather
1054 Overflows: An Excitation-Emission Matrix Parallel Factor Analysis Assessment, Environ. Sci.
1055 Technol., 51, 1157-1167, <https://doi.org/10.1021/acs.est.6b03727>, 2017a.

1056 Chen, Q., Ikemori, F., and Mochida, M.: Light Absorption and Excitation-Emission Fluorescence
1057 of Urban Organic Aerosol Components and Their Relationship to Chemical Structure,
1058 Environ. Sci. Technol., 50, 10859-10868, <https://doi.org/10.1021/acs.est.6b02541>, 2016a.

1059 Chen, Q., Miyazaki, Y., Kawamura, K., Matsumoto, K., Coburn, S., Volkamer, R., Iwamoto, Y.,
1060 Kagami, S., Deng, Y., Ogawa, S., Ramasamy, S., Kato, S., Ida, A., Kajii, Y., and Mochida, M.:
1061 Characterization of Chromophoric Water-Soluble Organic Matter in Urban, Forest, and
1062 Marine Aerosols by HR-ToF-AMS Analysis and Excitation-Emission Matrix Spectroscopy,
1063 Environ. Sci. Technol., 50, 10351-10360, <https://doi.org/10.1021/acs.est.6b01643>, 2016b.

1064 Chen, Q., Ikemori, F., Nakamura, Y., Vodicka, P., Kawamura, K., and Mochida, M.: Structural and
1065 Light-Absorption Characteristics of Complex Water-Insoluble Organic Mixtures in Urban
1066 Submicrometer Aerosols, Environ. Sci. Technol., 51, 8293-8303,
1067 <https://doi.org/10.1021/acs.est.7b01630>, 2017b.

1068 [Chen, Q., Mu, Z., Song, W., Wang, Y., Yang, Z., Zhang, L., and Zhang, Y. L.: Size - Resolved](#)
1069 [Characterization of the Chromophores in Atmospheric Particulate Matter From a Typical](#)
1070 [Coal - Burning City in China, Journal of Geophysical Research: Atmospheres, 124,](#)
1071 [10546-10563, https://doi.org/10.1029/2019jd031149, 2019.](#)

1072 Chen, Y., Sheng, G., Bi, X., Feng, Y., Bixian Mai, A., and Fu, J.: Emission Factors for
1073 Carbonaceous Particles and Polycyclic Aromatic Hydrocarbons from Residential Coal
1074 Combustion in China, Environ. Sci. Technol., 39, 1861-1867,
1075 <https://doi.org/10.1021/es0493650>, 2005.

1076 [Chen, Y., and Bond, T. C.: Light absorption by organic carbon from wood combustion, Atmos.](#)
1077 [Chem. Phys., 10, 1773-1787, 10.5194/acp-10-1773-2010, 2010.](#)

1078 ~~Chen, Y., and Bond, T. C.: Light absorption by organic carbon from wood combustion, Atmos.~~
1079 ~~Chem. Phys., 10, 1773-1787, https://doi.org/10.5194/acp-10-1773-2010, 2009.~~

1080 [Chen, Y., Tian, C., Feng, Y., Zhi, G., Li, J., and Zhang, G.: Measurements of emission factors of](#)
1081 [PM_{2.5}, OC, EC, and BC for household stoves of coal combustion in China, Atmos. Environ.,](#)
1082 [109, 190-196, https://doi.org/10.1016/j.atmosenv.2015.03.023, 2015.](#)

1083 Chen, Y., Ge, X., Chen, H., Xie, X., Chen, Y., Wang, J., Ye, Z., Bao, M., Zhang, Y., and Chen, M.:
1084 Seasonal light absorption properties of water-soluble brown carbon in atmospheric fine
1085 particles in Nanjing, China, Atmos. Environ., 230-240,
1086 <https://doi.org/10.1016/j.atmosenv.2018.06.002>, 2018.

1087 [Cheng, Y., He, K. B., Zheng, M., Duan, F. K., Du, Z. Y., Ma, Y. L., Tan, J. H., Yang, F. M., Liu, J.](#)
1088 [M., Zhang, X. L., Weber, R. J., Bergin, M. H., and Russell, A. G.: Mass absorption efficiency](#)

1089 [of elemental carbon and water-soluble organic carbon in Beijing, China, Atmos. Chem. Phys.,](#)
1090 <https://doi.org/11,11497-11510,10.5194/acp-11-11497-2011>, 2011.

1091 [Cheng, Y., He, K.-b., Du, Z.-y., Engling, G., Liu, J.-m., Ma, Y.-l., Zheng, M., and Weber, R. J.: The](#)
1092 [characteristics of brown carbon aerosol during winter in Beijing, Atmos. Environ., 127,](#)
1093 [355-364, https://doi.org/10.1016/j.atmosenv.2015.12.035](https://doi.org/10.1016/j.atmosenv.2015.12.035), 2016.

1094 Coble, P. G.: Characterization of marine and terrestrial DOM in seawater using
1095 excitation-emission matrix spectroscopy, Mar. Chem., 51, 325-346,
1096 [https://doi.org/10.1016/0304-4203\(95\)00062-3](https://doi.org/10.1016/0304-4203(95)00062-3), 1996.

1097 [Coggon, M. M., Veres, P. R., Yuan, B., Koss, A., Warneke, C., Gilman, J. B., Lerner, B. M.,](#)
1098 [Peischl, J., Aikin, K. C., Stockwell, C. E., Hatch, L. E., Ryerson, T. B., Roberts, J. M.,](#)
1099 [Yokelson, R. J., and de Gouw, J. A.: Emissions of nitrogen-containing organic compounds](#)
1100 [from the burning of herbaceous and arboraceous biomass: Fuel composition dependence and](#)
1101 [the variability of commonly used nitrile tracers, Geophys. Res. Lett., 43, 9903-9912,](#)
1102 [10.1002/2016gl070562](https://doi.org/10.1002/2016gl070562), 2016.

1103 Cory, R. M., and Mcknight, D. M.: Fluorescence Spectroscopy Reveals Ubiquitous Presence of
1104 Oxidized and Reduced Quinones in Dissolved Organic Matter, Environ. Sci Technol., 39,
1105 8142-8149, <https://doi.org/10.1021/es0506962>, 2005.

1106 Cui, M., Chen, Y., Zheng, M., Li, J., Tang, J., Han, Y., Song, D., Yan, C., Zhang, F., Tian, C., and
1107 Zhang, G.: Emissions and characteristics of particulate matter from rainforest burning in the
1108 Southeast Asia, Atmos. Environ., 191, 194-204,
1109 <https://doi.org/10.1016/j.atmosenv.2018.07.062>, 2018.

1110 [Dasari, S., Andersson, A., Bikkina, S., Holmstrand, H., Budhavant, K., Satheesh, S. K., Asmi, E.,](#)
1111 [Kesti, J., Backman, J., and Salam, A.: Photochemical degradation affects the light absorption](#)
1112 [of water-soluble brown carbon in the South Asian outflow, Science Advances, 5,](#)
1113 <https://doi.org/10.1126/sciadv.aau8066>, 2019.

1114 [Dai, S., Bi, X., Chan, L. Y., He, J., Wang, B., Wang, X., Peng, P., Sheng, G., and Fu, J.: Chemical](#)
1115 [and stable carbon isotopic composition of PM_{2.5} from on road vehicle emissions in the PRD](#)
1116 [region and implications for vehicle emission control policy, Atmos. Chem. Phys., 15,](#)
1117 [3097-3108, https://doi.org/10.5194/acp-15-3097-2015](https://doi.org/10.5194/acp-15-3097-2015), 2015.

1118 [Di Lorenzo, R. A., Washenfelder, R. A., Attwood, A. R., Guo, H., Xu, L., Ng, N. L., Weber, R. J.,](#)

1119 [Baumann, K., Edgerton, E., and Young, C. J.: Molecular-Size-Separated Brown Carbon](#)
1120 [Absorption for Biomass-Burning Aerosol at Multiple Field Sites, Environ. Sci. Technol.,](#)
1121 <https://doi.org/10.1021/acs.est.6b06160>, 2017.

1122 Fan, X., Song, J., and Peng, P. a.: Comparison of isolation and quantification methods to measure
1123 humic-like substances (HULIS) in atmospheric particles, Atmos. Environ., 60, 366-374,
1124 <https://doi.org/10.1016/j.atmosenv.2012.06.063>, 2012.

1125 Fan, X., Wei, S., Zhu, M., Song, J., Peng, P: Comprehensive characterization of humic-like
1126 substances in smoke PM2.5 emitted from the combustion of biomass materials and fossil
1127 fuels, Atmos. Chem. Phys., 16, 13321-13340, <https://doi.org/10.5194/acp-16-13321-2016>,
1128 2016.

1129 Feng, S., Zhang, L., Wang, S., Nadykto, A. B., Xu, Y., Shi, Q., Jiang, B., and Qian, W.:
1130 Characterization of dissolved organic nitrogen in wet deposition from Lake Erhai basin by
1131 using ultrahigh resolution FT-ICR mass spectrometry, Chemosphere, 156, 438-445,
1132 <https://doi.org/10.1016/j.chemosphere.2016.04.039>, 2016.

1133 Feng, Y., Ramanathan, V., and Kotamarthi, V. R.: Brown carbon: a significant atmospheric
1134 absorber of solar radiation?, Atmos. Chem. Phys., 13, 8607-8621,
1135 <https://doi.org/10.5194/acp-13-8607-2013>, 2013.

1136 [Fleming, L. T., Lin, P., Laskin, A., Laskin, J., Weltman, R., Edwards, R., Arora, N. K., Yadav, A.,](#)
1137 [Meinardi, S., and Blake, D. R.: Molecular Composition of Particulate Matter Emissions from](#)
1138 [Dung and Brushwood Burning Household Cookstoves in Haryana, India, Atmos. Chem.](#)
1139 [Phys., 18, 2461-2480, https://doi.org/10.5194/acp-18-2461-2018, 2017.](#)

1140 Fu, P., Kawamura, K., Chen, J., Qin, M., Ren, L., Sun, Y., Wang, Z., Barrie, L. A., Tachibana, E.,
1141 Ding, A., and Yamashita, Y.: Fluorescent water-soluble organic aerosols in the High Arctic
1142 atmosphere, Sci Rep, 5, 9845, <https://doi.org/10.1038/srep09845>, 2015.

1143 [Gentner, D. R., Jathar, S. H., Gordon, T. D., Bahreini, R., Day, D. A., El Haddad, I., Hayes, P. L.,](#)
1144 [Pieber, S. M., Platt, S. M., de Gouw, J., Goldstein, A. H., Harley, R. A., Jimenez, J. L., Prevot,](#)
1145 [A. S., and Robinson, A. L.: Review of Urban Secondary Organic Aerosol Formation from](#)
1146 [Gasoline and Diesel Motor Vehicle Emissions, Environ. Sci. Technol., 51, 1074-1093,](#)
1147 <https://doi.org/10.1021/acs.est.6b04509>, 2017.

1148 [Ghidotti, M., Fabbri, D., Masek, O., Mackay, C. L., Montalti, M., and Hornung, A.: Source and](#)

1149 [Biological Response of Biochar Organic Compounds Released into Water; Relationships with](#)
1150 [Bio-Oil Composition and Carbonization Degree, Environ. Sci. Technol., 51, 6580-6589,](#)
1151 [https://doi.org/10.1021/acs.est.7b00520, 2017.](#)
1152 [Graber, E. R., and Rudich, Y.: Atmospheric HULIS: How humic-like are they? A comprehensive](#)
1153 [and critical review, Atmos. Chem. Phys., 6, 729-753, https://doi.org/10.5194/acp-6-729-2006,](#)
1154 [2006.](#)
1155
1156 Gu, Q., and Kenny, J. E.: Improvement of Inner Filter Effect Correction Based on Determination
1157 of Effective Geometric Parameters Using a Conventional Fluorimeter, Anal. Chem., 81,
1158 420-426, [https://doi.org/10.1021/ac801676j, 2009.](#)
1159 [Hecobian, A., Zhang, X., Zheng, M., Frank, N., Edgerton, E. S., and Weber, R. J.: Water-Soluble](#)
1160 [Organic Aerosol material and the light-absorption characteristics of aqueous extracts](#)
1161 [measured over the Southeastern United States, Atmos. Chem. Phys., 10, 5965-5977,](#)
1162 [https://doi.org/10.5194/acp-10-5965-2010, 2010.](#)
1163 Jiang, B., Kuang, B. Y., Liang, Y., Zhang, J., Huang, X. H. H., Xu, C., Yu, J. Z., and Shi, Q.:
1164 Molecular composition of urban organic aerosols on clear and hazy days in Beijing: a
1165 comparative study using FT-ICR MS, Environ. Chem., 13, 888-901,
1166 [https://doi.org/10.1071/en15230, 2016.](#)
1167 [Kahnt, A., Behrouzi, S., Vermeylen, R., Safi Shalamzari, M., Vercauteren, J., Roekens, E., Claeys,](#)
1168 [M., and Maenhaut, W.: One-year study of nitro-organic compounds and their relation to wood](#)
1169 [burning in PM10 aerosol from a rural site in Belgium, Atmos. Environ., 81, 561-568,](#)
1170 [https://doi.org/10.1016/j.atmosenv.2013.09.041, 2013.](#)
1171 Kirchstetter, T. W., and Thatcher, T. L.: Contribution of organic carbon to wood smoke particulate
1172 matter absorption of solar radiation, Atmos. Chem. Phys., 12, 5803-5816,
1173 [https://doi.org/10.5194/acp-12-6067-2012, 2012.](#)
1174 [Koch, B., and Dittmar, T.: Koch, B. P. & Dittmar, T. From mass to structure: An aromaticity index](#)
1175 [for high-resolution mass data of natural organic matter. Rapid Commun. Mass Spectrom. 20,](#)
1176 [926-932, Rapid Commun. Mass Spectrom., 20, 926-932, https://doi.org/10.1002/rcm.2386,](#)
1177 [2006.](#)
1178 [Kumar, N. K., Corbin, J. C., Bruns, E. A., Massabó, D., Slowik, J. G., Drinovec, L., Močnik, G.,](#)

1179 [Prati, P., Vlachou, A., Baltensperger, U., Gysel, M., El-Haddad, I., and Prévôt, A. S. H.:](#)
1180 [Production of particulate brown carbon during atmospheric aging of residential](#)
1181 [wood-burning emissions, Atmos. Chem. Phys., 18, 17843-17861,](#)
1182 <https://doi.org/10.5194/acp-18-17843-2018>, 2018.

1183 Laskin, A., Laskin, J., and Nizkorodov, S. A.: Chemistry of atmospheric brown carbon, Chem.
1184 Rev., 115, 4335-4382, <https://doi.org/10.1021/cr5006167>, 2015.

1185 [Laskin, A., Smith, J. S., and Laskin, J.: Molecular Characterization of Nitrogen-Containing](#)
1186 [Organic Compounds in Biomass Burning Aerosols Using High-Resolution Mass](#)
1187 [Spectrometry, Environ. Sci Technol., 43, 3764-3771, https://doi.org/10.1021/es803456n,](#)
1188 [2009.](#)

1189 Lee, H. J., Laskin, A., Laskin, J., and Nizkorodov, S. A.: Excitation-emission spectra and
1190 fluorescence quantum yields for fresh and aged biogenic secondary organic aerosols, Environ.
1191 Sci. Technol., 47, 5763-5770, <https://doi.org/10.1021/es400644c> 2013.

1192 [Li, C., He, Q., Schade, J., Passig, J., Zimmermann, R., Meidan, D., Laskin, A., and Rudich, Y.:](#)
1193 [Dynamic changes in optical and chemical properties of tar ball aerosols by atmospheric](#)
1194 [photochemical aging, Atmos. Chem. Phys., 19, 139-163,](#)
1195 <https://doi.org/10.5194/acp-19-139-2019>, 2019.

1196 Li, M., Fan, X., Zhu, M., Zou, C., Song, J., Wei, S., Jia, W., and Peng, P.: Abundances and light
1197 absorption properties of brown carbon emitted from residential coal combustion in China,
1198 Environ. Sci. Technol., 53, 595-603, <https://doi.org/10.1021/acs.est.8b05630>, 2018.

1199 [Lin, P., Rincon, A. G., Kalberer, M., and Yu, J. Z.: Elemental composition of HULIS in the Pearl](#)
1200 [River Delta Region, China: results inferred from positive and negative electrospray high](#)
1201 [resolution mass spectrometric data, Environ. Sci. Technol., 46, 7454-7462,](#)
1202 <https://doi.org/10.1021/es300285d>, 2012a.

1203 Lin, P., Yu, J. Z., Engling, G., and Kalberer, M.: Organosulfates in humic-like substance fraction
1204 isolated from aerosols at seven locations in East Asia: a study by ultra-high-resolution mass
1205 spectrometry, Environ. Sci. Technol., 46, 13118-13127, <https://doi.org/10.1021/es303570v>,
1206 2012b.

1207 [Lin, P., Aiona, P. K., Li, Y., Shiraiwa, M., Laskin, J., Nizkorodov, S. A., and Laskin, A.: Molecular](#)
1208 [Characterization of Brown Carbon in Biomass Burning Aerosol Particles, Environ. Sci.](#)

1209 [Technol., 50, 11815–11824, https://doi.org/10.1021/acs.est.6b03024, 2016.](https://doi.org/10.1021/acs.est.6b03024)

1210 [Lin, P., Aiona, P. K., Li, Y., Shiraiwa, M., Laskin, J., Nizkorodov, S. A., and Laskin, A.: Molecular](https://doi.org/10.1021/acs.est.6b03024)

1211 [Characterization of Brown Carbon in Biomass Burning Aerosol Particles, Environ. Sci.](https://doi.org/10.1021/acs.est.6b03024)

1212 [Technol., 50, 11815–11824, https://doi.org/10.1021/acs.est.6b03024, 2016.](https://doi.org/10.1021/acs.est.6b03024)

1213 Lin, P., Fleming, L. T., Nizkorodov, S. A., Laskin, J., and Laskin, A.: Comprehensive Molecular

1214 Characterization of Atmospheric Brown Carbon by High Resolution Mass Spectrometry with

1215 Electrospray and Atmospheric Pressure Photoionization, *Anal. Chem.*, 90, 12493–12502,

1216 [https://doi.org/10.1021/acs.analchem.8b02177, 2018.](https://doi.org/10.1021/acs.analchem.8b02177)

1217 [Liu, J., Bergin, M., Guo, H., King, L., Kotra, N., Edgerton, E., and Weber, R. J.: Size-resolved](https://doi.org/10.5194/acp-13-12389-2013)

1218 [measurements of brown carbon in water and methanol extracts and estimates of their](https://doi.org/10.5194/acp-13-12389-2013)

1219 [contribution to ambient fine-particle light absorption, Atmos. Chem. Phys., 13, 12389–12404,](https://doi.org/10.5194/acp-13-12389-2013)

1220 [https://doi.org/10.5194/acp-13-12389-2013, 2013.](https://doi.org/10.5194/acp-13-12389-2013)

1221 [Liu, J., Mo, Y., Ding, P., Li, J., Shen, C., and Zhang, G.: Dual carbon isotopes \(¹⁴C and ¹³C\)](https://doi.org/10.1016/j.scitotenv.2018.03.293)

1222 [and optical properties of WSOC and HULIS-C during winter in Guangzhou, China, Sci. Total](https://doi.org/10.1016/j.scitotenv.2018.03.293)

1223 [Environ., 633, 1571–1578, https://doi.org/10.1016/j.scitotenv.2018.03.293, 2018.](https://doi.org/10.1016/j.scitotenv.2018.03.293)

1224 Luciani, X., Mounier, S., Redon, R., and Bois, A.: A simple correction method of inner filter

1225 effects affecting FEEM and its application to the PARAFAC decomposition, *Chemom. Intell.*

1226 *Lab. Syst.*, 96, 227–238, [https://doi.org/10.1016/j.chemolab.2009.02.008, 2009.](https://doi.org/10.1016/j.chemolab.2009.02.008)

1227 [Lv, J., Zhang, S., Wang, S., Luo, L., Cao, D., and Christie, P.: Molecular-Scale Investigation with](https://doi.org/10.1021/acs.est.5b04996)

1228 [ESI-FT-ICR-MS on Fractionation of Dissolved Organic Matter Induced by Adsorption on](https://doi.org/10.1021/acs.est.5b04996)

1229 [Iron Oxyhydroxides, Environ. Sci. Technol., 50, 2328–2336,](https://doi.org/10.1021/acs.est.5b04996)

1230 [https://doi.org/10.1021/acs.est.5b04996, 2016.](https://doi.org/10.1021/acs.est.5b04996)

1231 Matos, J. T. V., Freire, S. M. S. C., Duarte, R. M. B. O., and Duarte, A. C.: Natural organic matter

1232 in urban aerosols: Comparison between water and alkaline soluble components using

1233 excitation–emission matrix fluorescence spectroscopy and multiway data analysis, *Atmos.*

1234 *Environ.*, 102, 1–10, [https://doi.org/10.1016/j.atmosenv.2014.11.042, 2015.](https://doi.org/10.1016/j.atmosenv.2014.11.042)

1235 [Mazzoleni, L. R., Ehrmann, B. M., Shen, X. H., Marshall, A. G., and Collett, J. L.: Water-Soluble](https://doi.org/10.1021/es903409k)

1236 [Atmospheric Organic Matter in Fog: Exact Masses and Chemical Formula Identification by](https://doi.org/10.1021/es903409k)

1237 [Ultrahigh-Resolution Fourier Transform Ion Cyclotron Resonance Mass Spectrometry,](https://doi.org/10.1021/es903409k)

1238 [Environ. Sci. Technol., 44, 3690–3697, https://doi.org/10.1021/es903409k, 2010.](https://doi.org/10.1021/es903409k)

1239 ~~Mo, Y., Li, J., Liu, J., Zhong, G., Cheng, Z., Tian, C., Chen, Y., and Zhang, G.: The influence of~~
1240 ~~solvent and pH on determination of the light absorption properties of water-soluble brown~~
1241 ~~carbon, Atmos. Environ., 161, 90-98, <https://doi.org/10.1016/j.atmosenv.2017.04.037>, 2017.~~

1242 Mo, Y., Li, J., Jiang, B., Su, T., Geng, X., Liu, J., Jiang, H., Shen, C., Ding, P., Zhong, G., Cheng,
1243 Z., Liao, Y., Tian, C., Chen, Y., and Zhang, G.: Sources, compositions, and optical properties
1244 of humic-like substances in Beijing during the 2014 APEC summit: Results from dual carbon
1245 isotope and Fourier-transform ion cyclotron resonance mass spectrometry analyses, Environ.
1246 Pollut., 239, 322-331, <https://doi.org/10.1016/j.envpol.2018.04.041>, 2018.

1247 ~~Mo, Y., Li, J., Liu, J., Zhong, G., Cheng, Z., Tian, C., Chen, Y., and Zhang, G.: The influence of~~
1248 ~~solvent and pH on determination of the light absorption properties of water-soluble brown~~
1249 ~~carbon, Atmos. Environ., 161, 90-98, <https://doi.org/10.1016/j.atmosenv.2017.04.037>, 2017.~~

1250 Murphy, K. R., Butler, K. D., Spencer, R. G., Stedmon, C. A., Boehme, J. R., and Aiken, G. R.:
1251 Measurement of dissolved organic matter fluorescence in aquatic environments: an
1252 interlaboratory comparison, Environ. Sci. Technol., 44, 9405-9412,
1253 <https://doi.org/10.1021/es102362t>, 2010.

1254 Murphy, K. R., Stedmon, C. A., Graeber, D., and Bro, R.: Fluorescence spectroscopy and
1255 multi-way techniques. PARAFAC, Anal. Methods, 5, 6557-6566,
1256 <https://doi.org/10.1039/c3ay41160e>, 2013.

1257 ~~Park, S., Yu, G.-H., and Lee, S.: Optical absorption characteristics of brown carbon aerosols~~
1258 ~~during the KORUS-AQ campaign at an urban site, Atmos. Res., 203, 16-27,~~
1259 ~~<https://doi.org/10.1016/j.atmosres.2017.12.002>, 2018.~~

1260 Park, S. S., and Yu, J.: Chemical and light absorption properties of humic-like substances from
1261 biomass burning emissions under controlled combustion experiments, Atmos. Environ., 136,
1262 114-122, <https://doi.org/10.1016/j.atmosenv.2016.04.022>, 2016.

1263 ~~Patriarea, C., Bergquist, J., Sjoberg, P. J. R., Tranvik, L., and Hawkes, J. A.: Online~~
1264 ~~HPLC-ESI-HRMS Method for the Analysis and Comparison of Different Dissolved Organic~~
1265 ~~Matter Samples, Environ. Sci. Technol., 52, 2091-2099,~~
1266 ~~<https://doi.org/10.1021/acs.est.7b04508>, 2018.~~

1267 Qin, J., Zhang, L., Zhou, X., Duan, J., Mu, S., Xiao, K., Hu, J., and Tan, J.: Fluorescence
1268 fingerprinting properties for exploring water-soluble organic compounds in PM 2.5 in an

1269 industrial city of northwest China, *Atmos. Environ.*, 184, 203-211,
1270 <https://doi.org/10.1016/j.atmosenv.2018.04.049>, 2018.

1271 ~~Riva, M., Tomaz, S., Cui, T. Q., Lin, Y. H., Perraudin, E., Gold, A., Stone, E. A., Villenave, E., and~~
1272 ~~Surratt, J. D.: Evidence for an Unrecognized Secondary Anthropogenic Source of~~
1273 ~~Organosulfates and Sulfonates: Gas Phase Oxidation of Polycyclic Aromatic Hydrocarbons~~
1274 ~~in the Presence of Sulfate Aerosol, *Environ. Sci. Technol.*, 49, 6654-6664,~~
1275 ~~<https://doi.org/10.1021/acs.est.5b00836>, 2015.~~

1276 Saleh, R., Robinson, E. S., Tkacik, D. S., Ahern, A. T., Liu, S., Aiken, A. C., Sullivan, R. C.,
1277 Presto, A. A., Dubey, M. K., Yokelson, R. J., Donahue, N. M., and Robinson, A. L.:
1278 Brownness of organics in aerosols from biomass burning linked to their black carbon content,
1279 *Nat. Geosci.*, 7, 647-650, <https://doi.org/10.1038/ngeo2220>, 2014.

1280 ~~Schmitt-Kopplin, P., Gelencser, A., Dabek-Zlotorzynska, E., Kiss, G., Hertkorn, N., Harir, M.,~~
1281 ~~Hong, Y., and Gebefugi, I.: Analysis of the Unresolved Organic Fraction in Atmospheric~~
1282 ~~Aerosols with Ultrahigh-Resolution Mass Spectrometry and Nuclear Magnetic Resonance~~
1283 ~~Spectroscopy: Organosulfates As Photochemical Smog Constituents, *Anal. Chem.*, 82,~~
1284 ~~[8017-8026](https://doi.org/10.1021/ac101444r), <https://doi.org/10.1021/ac101444r>, 2010~~

1285 Sgroi, M., Roccaro, P., Korshin, G. V., and Vagliasindi, F. G. A.: Monitoring the Behavior of
1286 Emerging Contaminants in Wastewater-Impacted Rivers Based on the Use of Fluorescence
1287 Excitation Emission Matrixes (EEM), *Environ. Sci. Technol.*, 51, 4306-4316,
1288 <https://doi.org/10.1021/acs.est.6b05785>, 2017.

1289 ~~Shetty, N. J., Pandey, A., Baker, S., Hao, W. M., and Chakrabarty, R. K.: Measuring light~~
1290 ~~absorption by freshly emitted organic aerosols: optical artifacts in traditional~~
1291 ~~solvent-extraction-based methods, *Atmos. Chem. Phys.*, 19, 8817-8830,~~
1292 ~~<https://doi.org/10.5194/acp-19-8817-2019>, 2019.~~

1293 Shimabuku, K. K., Kennedy, A. M., Mulhern, R. E., and Summers, R. S.: Evaluating Activated
1294 Carbon Adsorption of Dissolved Organic Matter and Micropollutants Using Fluorescence
1295 Spectroscopy, *Environ. Sci. Technol.*, 51, 2676-2684, <https://doi.org/10.1021/acs.est.6b04911>,
1296 2017.

1297 Sleighter, R. L., Chen, H., Wozniak, A. S., Willoughby, A. S., Caricasole, P., and Hatcher, P. G.:
1298 Establishing a measure of reproducibility of ultrahigh-resolution mass spectra for complex

1299 mixtures of natural organic matter, *Anal. Chem.*, 84, 9184-9191,
1300 <https://doi.org/10.1021/ac3018026>, 2012.

1301 [Smith, J. S., Laskin, A., and Laskin, J.: Molecular Characterization of Biomass Burning Aerosols](#)
1302 [Using High-Resolution Mass Spectrometry, *Anal. Chem.*, 81, 1512-1521, 2009.](#)

1303 Song, J., Li, M., Jiang, B., Wei, S., Fan, X., and Peng, P.: Molecular Characterization of
1304 Water-Soluble Humic like Substances in Smoke Particles Emitted from Combustion of
1305 Biomass Materials and Coal Using Ultrahigh-Resolution Electrospray Ionization Fourier
1306 Transform Ion Cyclotron Resonance Mass Spectrometry, *Environ. Sci. Technol.*, 52,
1307 2575-2585, <https://doi.org/10.1021/acs.est.7b06126>, 2018.

1308 [Song, J., Li, M., Fan, X., Zou, C., Zhu, M., Jiang, B., Yu, Z., Jia, W., Liao, Y., and Peng, P. a.:](#)
1309 [Molecular characterization of water- and methanol-soluble organic compounds emitted from](#)
1310 [residential coal combustion using ultrahigh-resolution electrospray ionization Fourier](#)
1311 [transform ion cyclotron resonance mass spectrometry, *Environ. Sci. Technol.*,](#)
1312 [<https://doi.org/10.1021/acs.est.9b04331>, 2019.](#)

1313 [Stubbins, A., Lapierre, J. F., Berggren, M., Prairie, Y. T., Dittmar, T., and del Giorgio, P. A.: What's](#)
1314 [in an EEM? Molecular signatures associated with dissolved organic fluorescence in boreal](#)
1315 [Canada, *Environ. Sci. Technol.*, 48, 10598-10606, <https://doi.org/10.1021/es502086e>, 2014.](#)

1316 Sun, H., Biedermann, L., and Bond, T. C.: Color of brown carbon: A model for ultraviolet and
1317 visible light absorption by organic carbon aerosol, *Geophys. Res. Lett.*, 34,
1318 <https://doi.org/10.1029/2007gl029797>, 2007.

1319 [Tao, S., Lu, X., Levac, N., Bateman, A. P., Nguyen, T. B., Bones, D. L., Nizkorodov, S. A., Laskin,](#)
1320 [J., Laskin, A., and Yang, X.: Molecular Characterization of Organosulfates in Organic](#)
1321 [Aerosols from Shanghai and Los Angeles Urban Areas by Nanospray-Desorption](#)
1322 [Electrospray Ionization High-Resolution Mass Spectrometry, *Environ. Sci. Technol.*, 48,](#)
1323 [10993-11001, <https://doi.org/10.1021/es5024674>, 2014.](#)

1324 Tian, J., Ni, H., Cao, J., Han, Y., Wang, Q., Wang, X., Chen, L. W. A., Chow, J. C., Watson, J. G.,
1325 Wei, C., Sun, J., Zhang, T., and Huang, R.: Characteristics of carbonaceous particles from
1326 residential coal combustion and agricultural biomass burning in China, *Atmos. Pollut. Res.*, 8,
1327 521-527, <https://doi.org/10.1016/j.apr.2016.12.006>, 2017.

1328 [Wang, Y., Hu, M., Lin, P., Guo, Q., Wu, Z., Li, M., Zeng, L., Song, Y., Zeng, L., Wu, Y., Guo, S.,](#)

1329 [Huang, X., and He, L.: Molecular Characterization of Nitrogen-Containing Organic](#)
1330 [Compounds in Humic-like Substances Emitted from Straw Residue Burning, Environ. Sci.](#)
1331 [Technol., 51, 5951-5961, <https://doi.org/10.1021/acs.est.7b00248>, 2017.](#)

1332 Wells, M. J. M., Mullins, G. A., Bell, K. Y., Da Silva, A. K., and Navarrete, E. M.: Fluorescence
1333 and Quenching Assessment (EEM-PARAFAC) of de Facto Potable Reuse in the Neuse River,
1334 North Carolina, United States, Environ. Sci. Technol., 51, 13592-13602,
1335 <https://doi.org/10.1021/acs.est.7b03766>, 2017.

1336 Wong, J. P. S., Nenes, A., and Weber, R. J.: Changes in Light Absorptivity of Molecular Weight
1337 Separated Brown Carbon Due to Photolytic Aging, Environ. Sci. Technol., 51, 8414-8421,
1338 <https://doi.org/10.1021/acs.est.7b01739>, 2017.

1339 [Wozniak, A. S., Bauer, J. E., Sleighter, R. L., Dickhut, R. M., and Hatcher, P. G.: Technical Note:](#)
1340 [Molecular characterization of aerosol-derived water soluble organic carbon using ultrahigh](#)
1341 [resolution electrospray ionization Fourier transform ion cyclotron resonance mass](#)
1342 [spectrometry, Atmos. Chem. Phys., 8, 5099-5111, <https://doi.org/10.5194/acp-8-5099-2008>,](#)
1343 [2008.](#)

1344 Wu, G., Ram, K., Fu, P., Wang, W., Zhang, Y., Liu, X., Stone, E. A., Pradhan, B. B., Dangol, P. M.,
1345 Panday, A. K., Wan, X., Bai, Z., Kang, S., Zhang, Q., and Cong, Z.: Water-Soluble Brown
1346 Carbon in Atmospheric Aerosols from Godavari (Nepal), a Regional Representative of South
1347 Asia, Environ. Sci. Technol., 53, 3471-3479, <https://doi.org/10.1021/acs.est.9b00596>, 2019.

1348 [Xie, M., Hays, M. D., and Holder, A. L.: Light-absorbing organic carbon from prescribed and](#)
1349 [laboratory biomass burning and gasoline vehicle emissions, Sci Rep, 7, 7318,](#)
1350 <https://doi.org/10.1038/s41598-017-06981-8>, 2017.

1351 [Xie, M., Chen, X., Holder, A. L., Hays, M. D., Lewandowski, M., Offenberg, J. H., Kleindienst, T.](#)
1352 [E., Jaoui, M., and Hannigan, M. P.: Light absorption of organic carbon and its sources at a](#)
1353 [southeastern U.S. location in summer, Environ. Pollut., 244, 38-46,](#)
1354 <https://doi.org/10.1016/j.envpol.2018.09.125>, 2019.

1355 Yan, C., Zheng, M., Sullivan, A. P., Bosch, C., Desyaterik, Y., Andersson, A., Li, X., Guo, X.,
1356 Zhou, T., Gustafsson, Ö., and Collett, J. L.: Chemical characteristics and light-absorbing
1357 property of water-soluble organic carbon in Beijing: Biomass burning contributions, Atmos.
1358 Environ., 121, 4-12, <https://doi.org/10.1016/j.atmosenv.2015.05.005>, 2015.

1359 Yan, G., and Kim, G.: Speciation and Sources of Brown Carbon in Precipitation at Seoul, Korea:
1360 Insights from Excitation-Emission Matrix Spectroscopy and Carbon Isotopic Analysis,
1361 Environ. Sci. Technol., 51, 11580-11587, <https://doi.org/10.1021/acs.est.7b02892>, 2017.

1362 Yassine, M. M., Dabek-Zlotorzynska, E., Harir, M., and Schmitt-Kopplin, P.: Identification of
1363 weak and strong organic acids in atmospheric aerosols by capillary electrophoresis/mass
1364 spectrometry and ultra-high-resolution Fourier transform ion cyclotron resonance mass
1365 spectrometry, Anal. Chem., 84, 6586-6594, <https://doi.org/10.1021/ac300798g>, 2012.

1366 Yu, H., Liang, H., Qu, F., Han, Z. S., Shao, S., Chang, H., and Li, G.: Impact of dataset diversity
1367 on accuracy and sensitivity of parallel factor analysis model of dissolved organic matter
1368 fluorescence excitation-emission matrix, Sci Rep, 5, 10207,
1369 <https://doi.org/10.1038/srep10207>, 2015.

1370 Zhang, X., Lin, Y. H., Surratt, J. D., Zotter, P., Prevot, A. S. H., and Weber, R. J.: Light -
1371 absorbing soluble organic aerosol in Los Angeles and Atlanta: A contrast in secondary
1372 organic aerosol, Geophys. Res. Lett., 38, <https://doi.org/10.1029/2011GL049385>, 2011.

1373 Zhang, X., Lin, Y. H., Surratt, J. D., and Weber, R. J.: Sources, composition and absorption
1374 Angstrom exponent of light-absorbing organic components in aerosol extracts from the Los
1375 Angeles Basin, Environ. Sci. Technol., 47, 3685-3693, <https://doi.org/10.1021/es305047b>,
1376 2013.

1377 Zhang, Y., Yuan, Q., Huang, D., Kong, S., Zhang, J., Wang, X., Lu, C., Shi, Z., Zhang, X., Sun, Y.,
1378 Wang, Z., Shao, L., Zhu, J., and Li, W.: Direct Observations of Fine Primary Particles From
1379 Residential Coal Burning: Insights Into Their Morphology, Composition, and Hygroscopicity,
1380 Journal of Geophysical Research: Atmospheres, 123, 12,964-912,979,
1381 <https://doi.org/10.1029/2018jd028988>, 2018.

1382 Zhao, Y., Hallar, A. G., and Mazzoleni, L. R.: Atmospheric organic matter in clouds: exact masses
1383 and molecular formula identification using ultrahigh-resolution FT-ICR mass spectrometry,
1384 Atmos. Chem. Phys., 13, 12343-12362, <https://doi.org/10.5194/acp-13-12343-2013>, 2013.

1385 Zhu, C. S., Cao, J. J., Huang, R. J., Shen, Z. X., Wang, Q. Y., and Zhang, N. N.: Light absorption
1386 properties of brown carbon over the southeastern Tibetan Plateau, Sci. Total Environ., 625,
1387 246-251, <https://doi.org/10.1016/j.scitotenv.2017.12.183>, 2018.

1388